Earth's Future

RESEARCH ARTICLE
10.1029/2023EF004370

Contributions of Tropical Cyclones and Atmospheric Rivers to Extreme Precipitation Trends Over the Northeast US

Bor-Ting Jong[1], **Hiroyuki Murakami**[2], **Thomas L. Delworth**[2], and **William F. Cooke**[2]

[1]Program in Atmospheric and Oceanic Sciences, Princeton University, Princeton, NJ, USA, [2]NOAA/OAR/Geophysical Fluid Dynamical Laboratory, Princeton, NJ, USA

Key Points:

- The autumn extreme precipitation trend over the Northeast US is primarily attributed to tropical cyclone-related events since the 1990s
- In future projections, extreme precipitation linked to atmospheric rivers increases faster than that associated with tropical cyclones
- Despite fewer projected tropical cyclones in the future, extreme precipitation associated with them is projected to increase

Supporting Information:

Supporting Information may be found in the online version of this article.

Correspondence to:

B.-T. Jong,
bor-ting.jong@noaa.gov

Citation:

Jong, B.-T., Murakami, H., Delworth, T. L., & Cooke, W. F. (2024). Contributions of tropical cyclones and atmospheric rivers to extreme precipitation trends over the Northeast US. *Earth's Future*, *12*, e2023EF004370. https://doi.org/10.1029/2023EF004370

Received 12 DEC 2023
Accepted 23 MAR 2024

Author Contributions:

Conceptualization: Bor-Ting Jong, Thomas L. Delworth
Data curation: Bor-Ting Jong, Hiroyuki Murakami, William F. Cooke
Formal analysis: Bor-Ting Jong
Funding acquisition: Thomas L. Delworth
Investigation: Bor-Ting Jong, Hiroyuki Murakami, Thomas L. Delworth
Methodology: Bor-Ting Jong, Hiroyuki Murakami
Project administration: Thomas L. Delworth
Resources: William F. Cooke
Software: Bor-Ting Jong

Abstract The Northeast United States (NEUS) has faced the most rapidly increasing occurrences of extreme precipitation within the US in the past few decades. Understanding the physics leading to long-term trends in regional extreme precipitation is essential but the progress is limited partially by the horizontal resolution of climate models. The latest fully coupled 25-km GFDL (Geophysical Fluid Dynamics Laboratory) SPEAR (**S**eamless system for **P**rediction and **EA**rth system **R**esearch) simulations provide a good opportunity to study changes in regional extreme precipitation and the relevant physical processes. Here, we focus on the contributions of changes in synoptic-scale events, including atmospheric rivers (AR) and tropical cyclone (TC)-related events, to the trend of extreme precipitation in the fall season over the Northeast US in both the recent past and future projections using the 25-km GFDL-SPEAR. In observations, increasing extreme precipitation over the NEUS since the 1990s is mainly linked to TC-related events, especially those undergoing extratropical transitions. In the future, both AR-related and TC-related extreme precipitation over the NEUS are projected to increase, even though the numbers of TCs in the North Atlantic are projected to decrease in the SPEAR simulations using the SSP5-8.5 projection of future radiative forcing. Factors such as enhancing TC intensity, strengthening TC-related precipitation, and/or westward shift in Atlantic TC tracks may offset the influence of declining Atlantic TC numbers in the model projections, leading to more frequent TC-related extreme precipitation over the NEUS.

Plain Language Summary In recent decades, the densely populated Northeast United States has faced the most rapid increase in the frequency of extreme rainfall within the US. Here, we examine the causes of the increase in extreme rainfall over the Northeast US in both current and future climates. We find that the surge in extreme rainfall since the 1990s is primarily linked to events associated with tropical cyclones. In a future warming climate, based on projections from a high-resolution climate model, our research shows that we can expect more frequent occurrences of extreme rainfall related to both atmospheric rivers and tropical cyclones. However, the increase in extreme rainfall linked to atmospheric rivers is projected to outpace that associated with tropical cyclones. Given the distinct spatial patterns of extreme rainfall resulting from atmospheric rivers and tropical cyclones, changes in their relative contributions could have profound implications for flood prevention and mitigation strategies.

1. Introduction

Extreme precipitation, both the intensity and frequency, has increased across much of the contiguous United States since the 20th century (e.g., Anderson et al., 2015; DeGaetano, 2009; Easterling et al., 2017; Hoerling et al., 2016; Janssen et al., 2014; Kunkel et al., 2013; Min et al., 2011). The Northeast US (NEUS; all acronyms used in this paper are listed in Table S1 in Supporting Information S1), the most populated region in North America including the Boston to DC metro corridor area, has experienced the most rapid increase in the frequency of extreme precipitation in the US, especially since the mid-1990s (e.g., Brown et al., 2010; Crossett et al., 2023; DeGaetano, 2009; DeGaetano et al., 2020; Frei et al., 2015; Guilbert et al., 2015; Hoerling et al., 2016; Howarth et al., 2019; Huang, Patricola, Winter, et al., 2021; Huang et al., 2017, 2018; Jong et al., 2023; Olafdottir et al., 2021). Extreme precipitation frequency over the NEUS, moreover, is projected to increase in the future warming climate (e.g., DeGaetano & Castellano, 2017; Hayhoe et al., 2007; Jong et al., 2023; Nazarian et al., 2022; Ning et al., 2015; Picard et al., 2023). In the face of warming climate and mounting threats from high-impact weather events such as extreme precipitation, long-term infrastructure development and planning depend on climate model future projections of these extreme events and their contributing meteorological processes.

Supervision: Thomas L. Delworth
Validation: Bor-Ting Jong
Visualization: Bor-Ting Jong
Writing – original draft: Bor-Ting Jong
Writing – review & editing: Bor-Ting Jong, Hiroyuki Murakami, Thomas L. Delworth, William F. Cooke

The trend of the NEUS extreme precipitation has been observed across all seasons, with the most pronounced trend occurring during the fall season (September-November) (Howarth et al., 2019; Huang et al., 2017; Kunkel et al., 2013). The NEUS extreme precipitation in the fall season is mostly provided by tropical cyclones (TCs), extratropical cyclones, and frontal systems (e.g., Agel et al., 2015, 2018; Barlow, 2011; Barlow et al., 2019; Huang et al., 2018; Kunkel et al., 2012; Smith et al., 2011). The increasing occurrence of extreme precipitation in the NEUS since the mid-1990s has been primarily attributed to TCs, with lesser influences from extratropical cyclones and frontal systems (e.g., Huang et al., 2018). Considering that moisture content and transport are critical to extreme precipitation (e.g., Barlow et al., 2019; Hsu & Chen, 2020; Teale & Robinson, 2020), other studies have also evaluated the contribution of atmospheric rivers (ARs), narrow corridors of intense atmospheric moisture transport, in comparison to TCs (Henny et al., 2022, 2023; Howarth et al., 2019). In these comparisons, TC-related events, including TC remnants, prior TC influences, and remote TC influences, are still the leading contributors to the increasing extreme precipitation frequency. The increase in TC influence is partly connected to the rising frequency of TCs in the North Atlantic since the 1990s (e.g., Huang et al., 2018; Murakami et al., 2020). The increase in TC frequency has been attributed to multiple factors, including a decrease in anthropogenic aerosol in the Western Hemisphere since the 1980s (e.g., Murakami, 2022; Wang et al., 2023) and a shift to the positive phase of the Atlantic Multidecadal Oscillation (AMO) (e.g., Huang et al., 2018; Murakami et al., 2020). Also, studies have shown that TC tracks in the North Atlantic have become more complex and slower moving in the past three decades. Slower-moving TCs are more likely to "stall" along the East Coast, subsequently amplifying their influence on extreme precipitation over the NEUS (e.g., Hall & Kossin, 2019; Henny et al., 2022). Furthermore, observed precipitation caused by TCs making landfall along the US East Coast has intensified, especially over land, in recent decades (e.g., Hallam et al., 2023; Touma et al., 2019). All in all, increases in NEUS extreme precipitation since the 1990s have been largely influenced by changes in the characteristics of TCs.

Multiple climate models have projected that extreme precipitation over the NEUS will increase in the future with global warming (e.g., DeGaetano & Castellano, 2017; Hayhoe et al., 2007; Jong et al., 2023; Nazarian et al., 2022; Ning et al., 2015; Picard et al., 2023). In recent work, Jong et al. (2023) used a high-resolution model (25 km horizontal grid) to show the frequency of extreme precipitation events in the fall season (defined as the top 1% of daily precipitation based upon the historical climatology for the 1951–2020 period) would double by the end of the 21st century. Very extreme precipitation (>150 mm/day), such as heavy rainfall related to hurricanes, may be six times more likely by 2100 compared to the early 21st century under the Shared Socioeconomic Pathway 5–8.5 (SSP5-8.5), high-end projection of future greenhouse gas emission (Jong et al., 2023). Furthermore, this study projects that the contribution of external anthropogenic forcing to increasing extreme precipitation would be distinguishable from the contribution of natural internal variability by the mid-21st century under the SSP5-8.5 scenario (Jong et al., 2023). While studies have agreed that the frequency of extreme precipitation will increase over the NEUS, there has been much less study of how different meteorological processes, such as ARs or TCs, would contribute to the increase in NEUS extreme events.

ARs are conducive to extreme precipitation over the NEUS in the fall season (e.g., Agel et al., 2015, 2018; Henny et al., 2022; Hsu & Chen, 2020; Slinskey et al., 2020; Teale & Robinson, 2020). In a future warmer climate, ARs are projected to become more frequent in many places across the globe, including eastern North America (e.g., Espinoza et al., 2018; O'Brien et al., 2022; Payne et al., 2020; Tseng et al., 2022; Zhao, 2020, 2022), since the increase in atmospheric moisture content in a warmer atmosphere overwhelms other factors such as change in circulations (e.g., Payne et al., 2020; and references therein). AR days over the NEUS in the fall season for the 2075–2100 period, under the representative concentration pathway 8.5 scenario (RCP8.5), are projected to be 2.3 times more frequent than those in the 1979–2008 period, in the 25-km GFDL High-Resolution Atmospheric Model (HiRAM) (Hsu & Chen, 2020). In addition, AR-related precipitation is expected to be more intense over the NEUS, as the increase in atmospheric moisture mostly follows the Clapeyron-Clausius scaling over regions with little topographic lift like the eastern US (e.g., Hsu & Chen, 2020; Payne et al., 2020; Zhao, 2022). How the changes in the AR frequency and AR-related precipitation will promote extreme precipitation over the NEUS in the warming climate, nevertheless, have not yet been established.

Projected changes in TC influence over the US East Coast are subject to a wide range of uncertainties. First of all, TC frequency in the North Atlantic is projected to decline in the future in the majority of climate model studies (e.g., Knutson et al., 2020; Roberts et al., 2020a, 2020b; and references therein). However, this projected decrease in TC frequency is still highly uncertain (e.g., Hsieh et al., 2022, 2023; Jing et al., 2021; Knutson et al., 2020; Lee

et al., 2023; Roberts et al., 2020b; Sobel et al., 2021; and references therein). For example, opposite results have been derived from some climate model projections (e.g., Bhatia et al., 2018; Murakami et al., 2014; Vecchi et al., 2019) and statistical-dynamical downscaling (e.g., Emanuel, 2013, 2021; Lee et al., 2020, 2022). On the other hand, studies have proposed that the proportion of TCs making landfall on the US East Coast, especially major hurricanes, would increase (e.g., Knutson et al., 2022; Liu et al., 2018; Wright et al., 2015), partially due to the TC genesis locations moving closer to the East Coast (Garner et al., 2021; Knutson et al., 2022) and change in large-scale steering flows (Knutson et al., 2022) in the future. Change in the large-scale environment has also been projected to modulate vertical wind shear near the US East Coast, favoring TC intensification near the US East Coast (Ting et al., 2019). Furthermore, TCs are projected to move slower along the US coast, lengthening the period of TC influences over land (e.g., Garner et al., 2021; Gori et al., 2022; Lee et al., 2022; Zhang et al., 2020). TC-related precipitation when TCs approach land is also projected to increase (e.g., Kitoh & Endo, 2019; Liu et al., 2018; Patricola & Wehner, 2018; Stansfield, Reed, & Zarzycki, 2020; Wright et al., 2015; Zhao, 2022). All these projected changes regarding the different aspects of TCs suggest that TCs would raise extreme precipitation risk over the NEUS, even though the TC frequency over the North Atlantic is projected to decline.

TCs threaten the NEUS region even after they move into the midlatitudes, becoming extratropical cyclones, a process known as extratropical transition (ET). For example, Hurricane Irene (2011; e.g., Jung & Lackmann, 2019; Liu et al., 2020; Liu & Smith, 2016) and Hurricane Sandy (2012; e.g., Evans et al., 2017; Galarneau et al., 2010) both brought hazardous extreme precipitation to the NEUS region during their ET phases. Studies using climate model projections have shown that in a future warming climate, a higher fraction of TCs would undergo ET (Baker et al., 2022; Michaelis & Lackmann, 2019). This implies that more cyclones originating from TCs and restrengthened would travel to the higher latitude region, enhancing the risk of extreme precipitation over regions that have experienced less events originating from TCs in the current climate. Also, ET-related precipitation is projected to intensify as the atmospheric moisture will be increased in a warmer climate (Jung & Lackmann, 2021, 2023; Liu et al., 2018, 2020). The projected change of other aspects of ETs, on the other hand, are still highly uncertain. For example, different climate models with horizontal resolutions finer than 50 km disagree on change in the future ET intensity. Also, climate models have shown less skill in simulating interannual variability in ETs than in TCs (Baker et al., 2022). These limitations suggest that it is still challenging to assess the changing contribution of ETs to extreme precipitation in the future warming climate.

Model resolution is one of the primary challenges in projecting changes in extreme precipitation and the relevant physical processes. Enhancing models' horizontal resolution to finer than 50 km has been shown to better simulate frequency of extreme precipitation, as more intense precipitation events can be permitted by the higher-resolution models (e.g., Iles et al., 2020; Kopparla et al., 2013; Lucas-Picher et al., 2017; Schiemann et al., 2018; Stansfield, Reed, Zarzycki, et al., 2020; Van der Wiel et al., 2016; Wehner et al., 2010, 2014). For example, in GFDL (Geophysical Fluid Dynamics Laboratory) SPEAR (**S**eamless system for **P**rediction and **EA**rth system **R**esearch) models with three different atmospheric horizontal resolution (100, 50, and 25 km), the 25-km SPEAR configuration simulates much more realistic frequency of extreme precipitation over the NEUS than the 50-km or 100-km SPEAR configurations (Jong et al., 2023). Also, models with finer resolutions can better represent several physical processes related to extreme precipitation including ARs and TCs. Many aspects of ARs are better resolved in models with higher resolutions (e.g., Hagos et al., 2016; Payne et al., 2020; Zhao, 2020), including atmospheric moisture transport over the ocean (e.g., Demory et al., 2014). Also, high-resolution climate models can facilitate simulation of AR-related precipitation since topography is much better represented in the models (e.g., Schiemann et al., 2018; Vannière et al., 2019). For TCs, coupled climate models with enhanced horizontal resolution to 25 km generally yield more frequent and stronger TCs, leading to better representations of the spectrum of TC intensities, compared to the same models with coarser resolutions (e.g., Camargo & Wing, 2016; Murakami et al., 2015; Reed & Chavas, 2015; Roberts et al., 2015, 2020a, 2020b; Shaevitz et al., 2014; Sobel et al., 2021). Additionally, TC tracks and genesis regions, especially for major hurricanes, and storm structures are much more realistic in models with 25 km resolution (e.g., Murakami et al., 2015; Roberts et al., 2020a, 2020b). On the other hand, fully coupled climate models incorporate local TC-ocean interactions which cools sea surface temperature along TC tracks due to strong TC winds, influencing the simulation of TC precipitation compared to uncoupled climate models (e.g., Huang, Patricola, & Collins, 2021). The latest fully coupled 25-km GFDL SPEAR ensemble, therefore, has paved the way for studying change in regional extreme precipitation and the relevant physical processes.

In this study, we focus on the changes in the synoptic-scale contributions, including ARs, TCs, and ETs, to extreme precipitation trend over the NEUS using the 25-km GFDL SPEAR. We first assess the performance of the model in the historical context. Then, we use the model to project the change in extreme precipitation over the NEUS as well as the changing contributions of the meteorological processes to the extreme precipitation trend.

2. Data and Method

2.1. Observational Data

For observational precipitation data, we use gridded daily precipitation data from National Oceanic and Atmospheric Administration (NOAA) Climate Prediction Center (CPC) Unified Gauge-Based Analysis which has resolution at 0.25deg by 0.25deg for the period of 1948–2022 (Chen et al., 2008). This data set has a high quality and small bias over the continental US according to previous evaluations (Sun et al., 2018) and has been chosen to assess the US extreme precipitation in historical simulations from the Coupled Model Intercomparison Project 6 (CMIP6) models (Akinsanola et al., 2020). For the NEUS extreme precipitation, specifically, this gridded data set also shows consistent temporal variations in extreme precipitation frequency for the period of 1948–2020 with station data (Global Historical Climatology Network Daily, Jong et al., 2023; Menne et al., 2012).

Variables used for AR and TC detections are derived from the 55-year Japanese Reanalysis Project (JRA-55; Kobayashi et al., 2015). JRA-55 provides 6-hourly atmospheric analysis fields at a 1.25° × 1.25° horizontal resolution from 1958 to 2023. JRA-55 is more ideal for TC detection than other reanalysis data sets, such as the latest high-resolution ECMWF Reanalysis v5 (ERA5; (Hersbach et al., 2020), since JRA-55 assimilation uses artificial wind retrievals in the vicinity of TCs. The wind retrievals incorporate TC wind profiles from best track data (Fiorino, 2002) and are processed like observed data (Hatsushika et al., 2006; Kobayashi et al., 2015). JRA-55 has demonstrated a lower false TC detection rate compared to other reanalysis data sets that did not assimilate observed TC information (Bieli et al., 2019; Murakami, 2014). For AR detection, we use vertically integrated vapor transport (IVT) from JRA-55. Climatological IVT from 1959 to 2020 in JRA-55 is highly similar to that of ERA5 (Figure S1 in Supporting Information S1).

2.2. Model Data

SPEAR is the latest coupled GCM from NOAA GFDL (Delworth et al., 2020). SPEAR uses similar component models as the GFDL Global Climate Model version 4 (CM4) (AM4 atmosphere and LM4 land model, Held et al., 2019; Zhao et al., 2018; MOM6 ocean and SIS2 sea ice models, Adcroft et al., 2019) but with configurations optimized for the study of seasonal to multidecadal variability, predictability, and projection.

SPEAR provides three options for horizontal resolution in the atmosphere and land components: 1° (∼100 km), 0.5° (∼50 km), and 0.25° (∼25 km). The physics are identical across these three configurations, with the exception of modest tuning in the damping, advection, and radiative parameters for the 25-km version to improve the simulation of TC intensity and maintain radiative balance. The model timesteps change with resolution for numerical stability. All configurations are coupled to the same 1° ocean model (with tropical refinement to 1/3°). We use the 25-km version of SPEAR, denoted as SPEAR_HI, in this study. The details of SPEAR's physical parameterizations and configurations can be found in Delworth et al. (2020). The comparisons of the three SPEAR resolutions in simulating the NEUS extreme precipitation are documented in Jong et al. (2023).

Here, we examine simulations with historical forcing and projected forcing following the SSP5-8.5 scenario. The historical simulations are driven by the observed time-evolving changes in radiative forcing agents (greenhouse gases, aerosols, land use, solar irradiance, and volcanic aerosols) over the period of 1921–2014. The SSP5-8.5 pathway represents a very high-end projection of future anthropogenic greenhouse gas emissions scenarios and covers the period of 2015–2100. It is worth being cautious that the SSP5-8.5 is sometimes considered an overestimate of projected future warming (e.g., Burgess et al., 2021; Hausfather & Peters, 2020). SPEAR_HI has 10 ensemble members for historical and SSP5-8.5 simulations. Each historical ensemble member was initialized from a 1,000-year Control run, starting from year 101 and with 20-year spacing to sample different phases of internal variability. Each member was run for the period of 1921–2014 with the historical forcing and extended to 2100 using the scenario forcings described above. The different realization of possible internal variability is represented by ensemble spread.

2.3. Method

2.3.1. The NEUS Region

The Northeast US (NEUS) region is defined as the US land territory within 37–50°N, 80.5–67°W, including the states of Maine, New Hampshire, Vermont, Massachusetts, Rhode Island, Connecticut, New York, New Jersey, Pennsylvania, Delaware, Maryland, Washington D.C., and parts of Virginia and West Virginia. Dashed-line boxes in Figure 6 indicate the area of the NEUS region. Canada and ocean regions are masked out.

2.3.2. Extreme Precipitation Days

As we attempt to connect extreme precipitation occurrences with synoptic weather events, we use extreme precipitation days based on the method from Henny et al. (2022) to filter out isolated extreme values. The procedure to derive extreme precipitation days is as below:

1. For each grid point, the extreme precipitation threshold is defined as daily accumulated precipitation falling in the 99th percentile (top 1%) of recorded wet days (≥0.1 mm/day) from September to November.
2. On each day, extreme precipitation across the NEUS is summed up. Days falling in the top 20% of this sum are defined as "extreme precipitation (EP) days."

The duration of any precipitation event is not taken into account in this study. Each day is treated independently. Also, this method may overlook some extreme events that occur overnight. Both the extreme precipitation threshold and EP days threshold are based upon the climatology from 1959 to 2020.

For SPEAR_HI, each ensemble member is processed independently: namely, each ensemble member has its own thresholds to select EP days.

2.3.3. AR Detection

ARs are identified by the detection algorithm from Mundhenk et al. (2016). This algorithm tests if the gridded daily IVT meets specific intensity and geometry (>1,400 km in length and with an aspect ratio ≥1.4) criteria that represent the plume-like nature of ARs across the globe. The IVT is defined as

$$\mathrm{IVT} = \frac{1}{g}\sqrt{\left(\int_{1000\mathrm{hPa}}^{250\mathrm{hPa}} uq\,dp\right)^2 + \left(\int_{1000\mathrm{hPa}}^{250\mathrm{hPa}} vq\,dp\right)^2}$$

where g is the gravitational acceleration, u is the zonal wind, v is the meridional wind, q is the specific humidity, and p is the pressure coordinate.

Following the previous studies (e.g., Mundhenk et al., 2018; Rutz et al., 2019; Tseng et al., 2022), we use the 94th percentile of global daily IVT anomalies over the period of 1959–2020 as the threshold. For SPEAR_HI, the same procedure is applied to each ensemble member. The algorithm does not track individual ARs over time, so each IVT map is examined independently. A daily AR mask is generated: 0 for non-AR and 1 for AR for each grid cell. This detection algorithm is compared to other AR detection algorithms within the Atmospheric River Tracking Method Intercomparison Project (ARTMIP). The comparisons show consistency in the frequency of ARs over the US, including both the west and east coasts, regardless of the threshold choices (O'Brien et al., 2022; Rutz et al., 2019). The detection algorithm is available online: https://mountainscholar.org/handle/10217/170619.

2.3.4. TC Tracking Scheme

We apply the same tracking scheme to both JRA-55 reanalysis data and SPEAR_HI, following the procedure detailed in Murakami et al. (2015). This scheme detects local minimum sea level pressure (SLP), closed contours of SLP about storm center, warm cores, distances of storm centers from tracks, and durations of warm core as well as wind exceeding minimum wind speed thresholds. The criteria for warm cores identification, distances of storm centers from tracks, and minimum wind speed are adjusted differently in JRA-55 and SPEAR_HI in order for the calculated annual total numbers of TCs across the globe to be similar to the observational number (~84). The tracking procedure and criteria for both JRA-55 and SPEAR_HI are detailed in Text S1 in Supporting

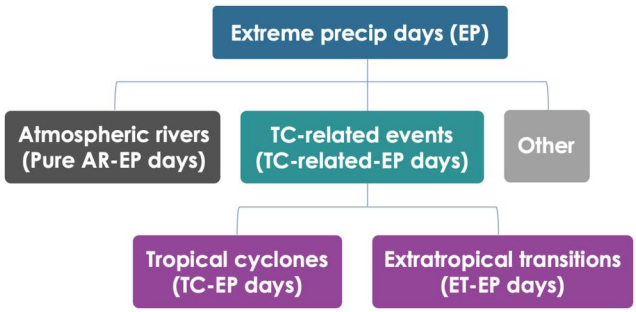

Figure 1. Schematic of the category procedure used to categorize EP days into different meteorological processes, including: EP days accompanied with TC-related events (TC-related-EP days), EP days accompanied with ARs only (pure AR-EP days), and EP days accompanied with neither TC-related nor ARs event (other).

Information S1. TC track density used in this study presents the TC frequency of occurrence counted for each 2.5° × 2.5° grid box.

2.3.5. ET Detection

Cyclone Phase Space (Hart, 2003) is employed to objectively identify cyclones that undergo ET. The Cyclone Phase Space consists of three parameters: the geopotential thickness (900–600 hPa) asymmetry across the storm (parameter, B), the upper-level (600–300 hPa) thermal wind (parameter $-V_T^U$) and the lower-level (900–600 hPa) thermal wind (parameter $-V_T^L$).

We follow Liu et al. (2017) using a simplified method to calculate the Cyclone Phase Space parameters because 6-hourly geopotential height from model outputs are available only at a few pressure levels. Rather than applying linear regression on geopotential heights at multiple isobaric levels to derive thermal winds used in the original method in Hart (2003), the thermal wind parameters are calculated from geopotential height at two isobaric levels: 500 and 850 hPa for $-V_T^L$; 300 and 500 hPa for $-V_T^U$. The parameter B is computed as the thermal thickness difference between 850 and 500 hPa. More details of the simplified Cyclone Phase Space and the assessment of its suitability can be found in Liu et al. (2017) and Bieli et al. (2020). Following Liu et al. (2017), ET onset is the first time a TC is either asymmetric ($B > 10$ m) or has a cold core ($-V_T^L < 0$), and ET completion is when both conditions are satisfied. For consistency, the same simplified method is also applied to the Cyclone Phase Space parameters in JRA-55.

In SPEAR_HI future projection analyses, we consistently use the same thresholds and criteria to define EP days, ARs, TCs, and ETs based upon the 1959–2020 climatology. As most of the current infrastructure has been built upon the current climate, using the same historical thresholds can give us a better sense how extreme precipitation and the resulting risk will change compared to the current climate.

2.3.6. Category Procedure

To assess different meteorological processes that may contribute to the increasing NEUS extreme precipitation, we decompose EP days into subcategories that include EP days accompanied with TC-related events (TC-related-EP days), EP days accompanied with ARs only (pure AR-EP days), and EP days accompanied with neither TC-related nor ARs event (other). A schematic of this category procedure is shown in Figure 1.

1. TC-related-EP days:
   For any given EP day, if there is at least one TC-related event with its center located within 1,000 km of the NEUS region, that EP day is considered as a "TC-related-EP day." TC-related events include both TCs and ETs (an extratropical cyclone transitioned from a TC). We also examine the contributions of TCs and ETs separately, denoted as "TC-EP days" and "ET-EP days." The sum of TC-EP days and ET-EP days equals to TC-related-EP days. Rather than 500 km as used in many previous studies (e.g., Henny et al., 2022; Huang et al., 2018), we choose 1,000 km because a TC-related event can often bring extreme precipitation to the NEUS even from a remote distance (e.g., Henny et al., 2022; Howarth et al., 2019) if the TC-related event interacts with or merges into pre-existing intense extratropical moisture (e.g., predecessor rain events in Galarneau et al., 2010).
   The TC tracking and ET detection data have a six-hourly temporal resolution and can record the phase change of a cyclone. In other words, this could record a TC experiencing transition into ET during a day. To account for this, we treat each six-hourly time-step as 0.25 TC and ET days.
2. Pure AR-EP days:
   For any given EP day, if an AR is detected in the NEUS region and there are no TC-related events tracked within 1,000 km of the NEUS, we categorize it as a "pure AR-EP day."
3. Other:
   Any EP days that are not categorized into TC-related-EP days or pure AR-EP days are aggregated into "Other." Only about 15% of the observational EP days from 1959 to 2020 fall into this category (Table 1). That is, the majority of EP days in the NEUS in the fall season are caused by either TC-related events and/or ARs.

Table 1
The Percentage of Days With Each Meteorological Processes Relative to the Total Number of Extreme Precipitation (EP) Days Over the (First Column) 1959 to 2020, (Second Column) 1959 to 1989, and (Third Column) 1990 to 2020 Periods, in Observations

Observations	1959–2020	1959–1989	1990–2020
Pure AR-EP days	58.0%	61.3%	55.8%
TC-related-EP days	27.2%	25.0%	28.8%
Other EP days	14.8%	13.7%	15.4%

The other types of meteorological factors include extratropical cyclones (without the presence of ARs), remnants of TCs, and intense mesoscale convective systems.

2.3.7. Statistical Significance

In this study, the statistical significance of differences between two periods is assessed using bootstrapping resampling. We first randomly shuffle the original time series and select two periods, with the same length of the test period, from the shuffled time series. Then, we calculate the differences between these two randomly selected periods. The procedure is repeated 1,000 times to evaluate the significance of the targeted differences.

3. Results

3.1. Changes in Observations/Reanalysis

In the NEUS, EP days in the fall season are predominantly associated with ARs and/or TC-related events and their occurrences have increased statistically significantly since the 1990s in observations. 58% of the EP days from 1959 to 2020 are accompanied solely by ARs (i.e., there is no TC-related event occurring within 1,000 km of the NEUS region); while 27% of EP days are accompanied by TC-related events (TC-related-EP days), indicating the presence of either TC and/or ET within 1,000 km of the NEUS region (Table 1; first column). This relative contribution of TCs to extreme precipitation aligns with the numbers reported by previous studies (e.g., 36% in Kunkel et al. (2012); 48% for September-October extreme precipitation in Huang et al. (2018); 28.3% in Henny et al. (2022)). Of the 57 TC-related-EP days in 1961–2020, 48 have concurrent ARs present in the NEUS region. In contrast, only about half of the 920 TC-related days see concurrent ARs (Table 2, first column). This suggests that TC-related events interacting with extratropical ARs can facilitate synoptic scale intense precipitation across the NEUS region, compared to TC-related events alone.

EP days in the NEUS have become much more frequent in the last three decades. Specifically, the total number of EP days from 1990 to 2020 is 41% more than the EP days observed from 1959 to 1989 (Figure 2a). The difference in the EP days between these two periods is statistically significant at the 95% confidence interval using the bootstrapping method. The relative contributions of ARs and TC-related events to the increases in EP days in the NEUS will be discussed next.

To assess the contribution of ARs to the increased NEUS EP days, Figure 2b presents the time series of the number of EP days accompanied purely by ARs (referred to as "pure AR-EP days") each year in observations. Comparing the periods of 1990–2020 and 1959–1989, we find that the number of pure AR-EP days has increased by 29%, but the difference is not statistically significant at the 90% confidence interval. The insignificant change in the pure AR-EP days may be related to the fact that both the number of ARs over the NEUS and the intensity of AR-related precipitation have not experienced substantial increase over the past three decades (Figures 3a and 3d). Further, the percentage of EP days exclusively associated with ARs has dropped from 61.3% in the period of

Table 2
(First Row) the Total Number of Days That There Are TC-Related Events Within 1,000 km From the NEUS Region, (Second Row) the Number of TC-Related Days Without Any ARs in the NEUS Region, (Third Row) the Total Number of TC-Related-EP Days for the NEUS, and (Fourth Row) the Number of TC-Related-EP Days Without Any ARs in the NEUS Region, (Left Column) in Observations During the 1961 to 2020 Period, (Middle Column) in SPEAR_HI During the 1961 to 2020 Period, and (Right Column) in SPEAR_HI Projections During the 2041 to 2100 Period

	Observations 1961–2020	SPEAR_HI 1961–2020	SPEAR_HI 2041–2100
TC-related days	920	870.9 (779–959)	789.5 (709–897)
TC-related days & No ARs	449	455.2 (403–496)	234.2 (191–278)
TC-related-EP days	57	57.7 (43–69)	74.6 (65–100)
TC-related-EP days & No ARs	9	13.3 (9–19)	12 (7–20)

Note. Numbers in parentheses show the spread of the ensemble members.

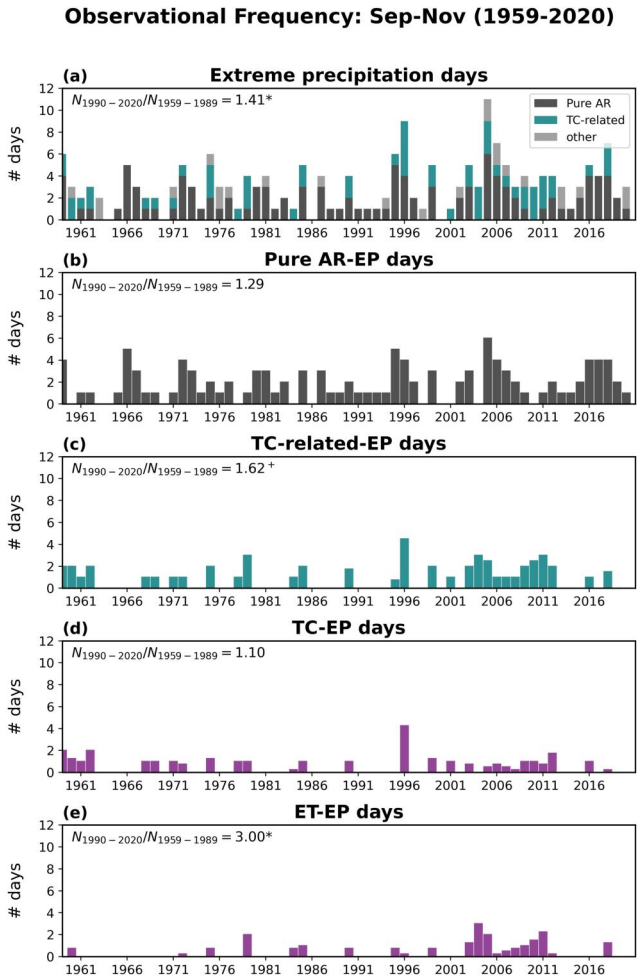

Figure 2. (a) Time-series for the number of extreme precipitation (EP) days over the NEUS in September-November in each year in observations from 1959 to 2020. The NEUS EP days are further categorized based upon the accompanied synoptic-scale meteorological factors: EP days accompanied by (b) ARs only (pure AR-EP days); (c) TC-related events (TCs and/or ETs; TC-related-EP days); (d) TCs (TC-EP days); and (e) ETs (ET-EP days). The numbers in each panel are the ratios between the total numbers of days in 1990–2020 versus the numbers in 1959–1989. Asterisks (crosses) indicate the differences between the two periods are statistically significant at the 95% (90%) confidence level.

1959–1989 to 55.8% in 1990–2020 (Table 1; top row), implying that the relative contribution of pure ARs to the NEUS EP days have declined in the recent decades. Collectively, ARs are not the primary contributor to the enhanced occurrences of EP days over the NEUS since the 1990s.

TC-related events, on the contrary, have played a dominant role in the enhanced occurrences of EP days over the NEUS since the 1990s. The total number of TC-related-EP days has surged by 60% from 1959–1989 to 1990–2020 (Figure 2c). This rise is also reflected in the percentage of EP days accompanied by TC-related days, which has grown from 25.0% in 1959–1989 to 28.8% in 1990–2020 (Table 1; middle row). This shows an increased relative contribution of TC-related events to extreme precipitation over the region. To further investigate how TC-related events have caused more frequent EP days, we decompose TC-related events into TCs and ETs (see Methods for more details; Figures 2d and 2e). The surge in EP days is mostly promoted by the amplified impacts of ETs, rather than by TCs. The total number of EP days accompanied by ETs only (ET-EP days) in 1990–2020 is three times the number in 1959–1989, whereas the total number of EP days accompanied by solely TCs (TC-EP days) remains similar between the two periods. Notably, the increased numbers of ET-EP days, are not attributable to the frequency of ETs as the number of ETs hitting the NEUS region does not exhibit a statistically significant increase since the 1990s in JRA-55 (Figure 3c). Precipitation intensity, instead, is the leading cause of the increased numbers of ET-EP days: the intensity of precipitation over the NEUS region when ETs are present has doubled in 1990–2020, compared to that in 1959–1989 (Figure 3f). This increase in ET precipitation intensity is statistically significant at the 95% confidence interval.

In brief, in observations, the increased extreme precipitation over the NEUS in the fall season is primarily attributed to the enhanced precipitation intensity related to ETs near the NEUS region. As a sensitivity test, we also used a 500 km distance threshold to select TC-relate-EP days over the NEUS, and this does not change the conclusion that ETs are the dominant contributor to the extreme precipitation trend over the NEUS (not shown). Next, we apply the same analysis to SPEAR_HI to assess the change in EP days and the contributions of ARs versus TC-related events to the EP days in the model's historical period.

3.2. Changes in SPEAR_HI Historical Simulations

In SPEAR_HI, EP days over the NEUS are also mostly associated with ARs and TC-related events as observed. Specifically, approximately 55% of EP days in 1959–2020 are accompanied purely by ARs within the NEUS region and roughly 30% of EP days are accompanied by TC-related events occurring within 1,000 km from the NEUS (Table 3, first column). These percentages are similar to the relative contributions to extreme precipitation as shown in observations (Table 1). Correspondingly, TC-related events that are concurrent with extratropical ARs can amplify the potential for synoptic scale intense precipitation across the NEUS region, compared to TC-related events alone. In the SPEAR_HI ensemble mean, only 13 out of the 58 TC-related-EP days are exclusively TC-related with no concurrent presence of ARs in the NEUS (Table 2, second column). EP days also have increased significantly in the recent three decades in SPEAR_HI: the total number of EP days in 1990–2020 is about 30% more than the number in 1959–1989, and the difference between the two periods is statistically significant at the 95% confidence interval (Figure 4a). For each ensemble member, the ratio of total EP days between 1990-2020 and 1959–1989 ranges from 0.98 to 1.71. Four (six) out of the 10 members simulate statistically significant increases in the later period at the 95% (90%) confidence levels, indicating a good agreement that the incidence of EP days has increased greatly in the later period.

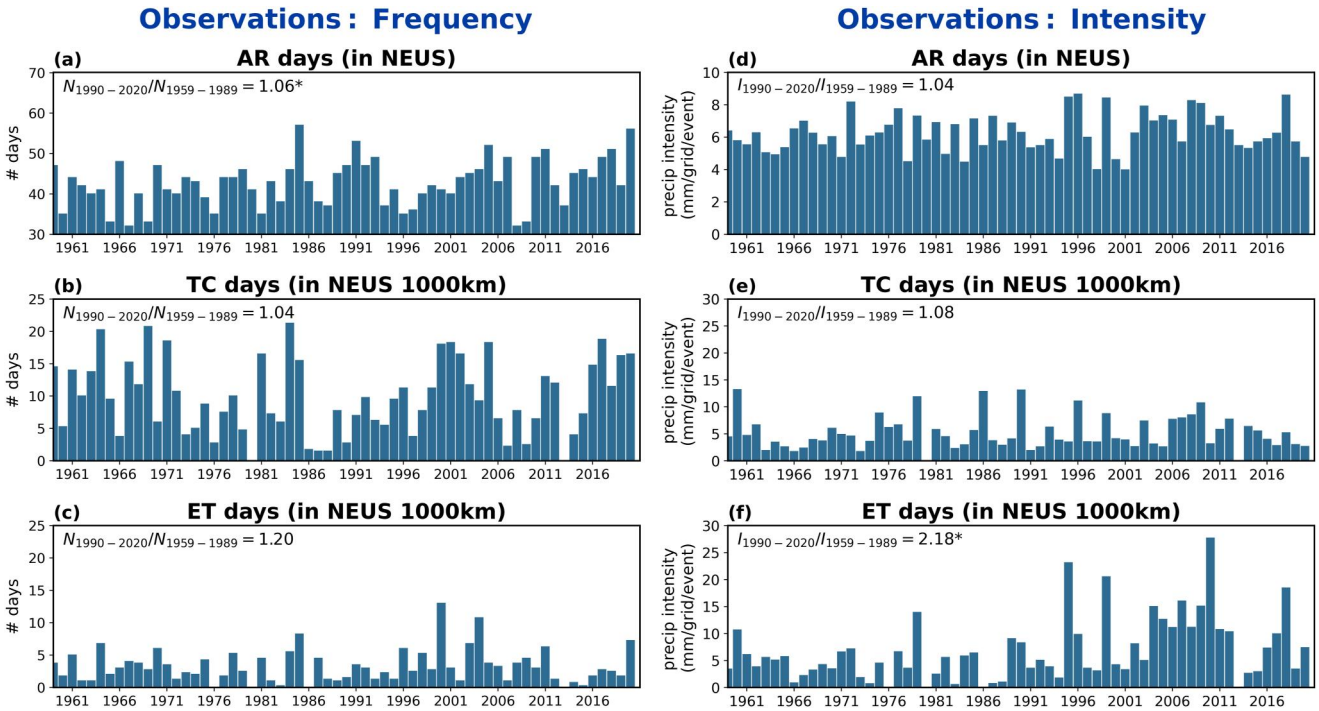

Figure 3. In observations, (left) the numbers of days that there are (a) ARs in the NEUS region; (b) TCs within 1,000 km from the NEUS; and (c) ETs within 1,000 km from the NEUS in September-November in each year. The numbers are the ratios between the total numbers of days in 1990–2020 versus the numbers in 1959–1989. (right) The average intensity of precipitation over the NEUS during (d) AR days; (e) TC days; and (f) ET days. The precipitation intensity is averaged over the numbers of grid points that record precipitation (>0.1 mm/day) during each event and the event numbers in each year. The unit of the precipitation intensity is mm/day. The numbers in the right panels are the average precipitation intensity over the NEUS in 1990–2020 versus the intensity in 1959–1989. Asterisks indicate the differences between the two periods are statistically significant at the 95% confidence level.

EP days accompanied purely by ARs increased significantly about 25% in the period of 1990–2020 compared to in 1959–1989, in SPEAR_HI (Figure 4b). This rise in pure AR-EP days may be linked to the slight increase in the number of AR days occurring in the NEUS region (Figure 5a): the total AR days in the NEUS region have enhanced about 10% in the later period. Conversely, the intensity of precipitation over the NEUS region when ARs are present remains similar (Figure 5d). Although the number of pure AR-EP days has increased significantly in the later period, the relative contribution of ARs to EP days has declined slightly from 57% in 1959–1989 to 54% in 1990–2020 (Table 3, top row). These comparisons imply that, in SPEAR_HI, the increase in AR frequency over the NEUS region may contribute marginally to the increased EP days. However, in general, ARs do not emerge as the dominant source driving the trend of extreme precipitation over the NEUS in the past three decades.

The increased EP days, on the other hand, are primarily driven by the increased influences from TC-related events. TC-related-EP days have surged by roughly 60% in the period of 1990–2020 compared to the number

Table 3
The Percentage of Days With Each Meteorological Processes Relative to the Total Number of EP Days Over the (First Column) 1959 to 2020, (Second Column) 1959 to 1989, (Third Column) 1990 to 2020, and (Fourth Column) 2041 to 2100 Periods, in SPEAR_HI Historical and SSP5-8.5 Simulations

SPEAR_HI	1959–2020	1959–1989	1990–2020	2041–2100
Pure AR-EP days	55.5% (47.9%–61.2%)	56.9% (45.7%–63.1%)	54.3% (44.9%–59.6%)	66.1% (62.3%–68.6%)
TC-related-EP days	28.6% (24.0%–33.4%)	25.1% (19.9%–31.4%)	31.3% (24.7%–37.6%)	21.5% (19.2%–28.3%)
Other EP days	15.9% (12.6%–21.1%)	18.0% (11.3%–32.5%)	14.4% (8.9%–19.4%)	12.4% (9.4%–15.0%)

Note. Numbers in parentheses show the spread of the ensemble members.

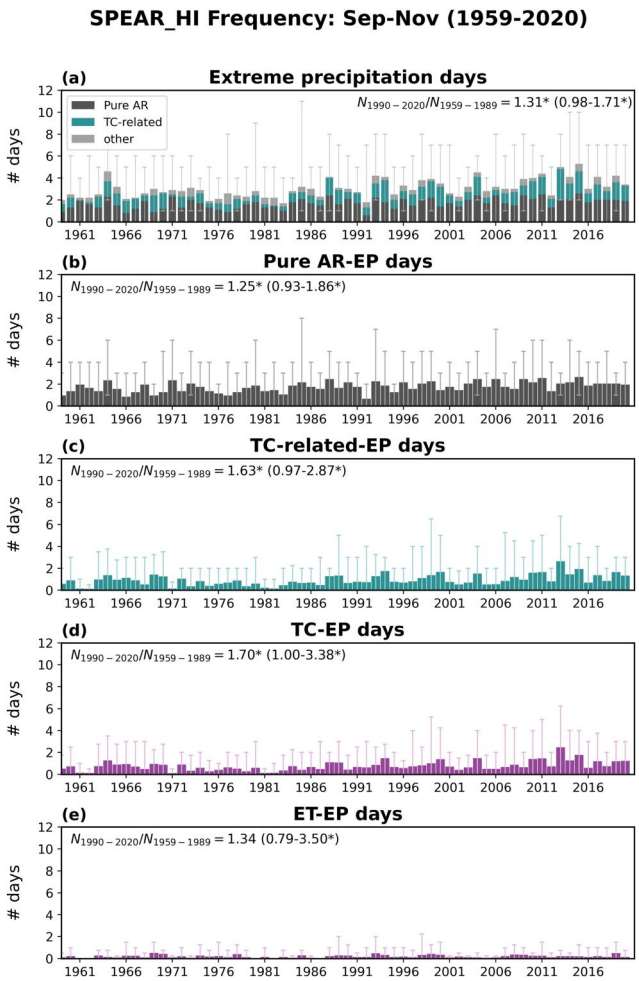

Figure 4. Same as Figure 2, but for SPEAR_HI ensemble simulations. Bars are the ensemble mean of SPEAR_HI. Thin lines indicate the spread across the 10 ensemble members. The ratio numbers in the parentheses are the range of the ratios from each ensemble member.

in 1959–1989 (Figure 4c). For individual ensemble members, the ratio of total TC-related-EP days between the two periods ranges from 0.97 to 2.87, suggesting that the majority of ensemble members agree on the sign of changes in TC-related-EP days. In addition, four (six) out of the 10 members simulate statistically significant increases in the later period at the 95% (90%) confidence levels. The percentage of EP days associated with TC-related events increases from about 25% in the period of 1959–1989 to about 31% in 1990–2020 (Table 3, middle row), supporting the increased relative contribution of TC-related events to the overall trend of extreme precipitation.

The contribution of TC-related events in SPEAR_HI is further decomposed into the contribution from TCs versus from ETs (Figures 4d and 4e). TC-EP days are 70% more frequent in the later period. Across individual ensemble members, the ratio of the frequency between these two periods ranges from 1 to 3.38 and five out of the 10 members simulate statistically significant increases in the later period at the 95% confidence levels, indicating a consensus among all ensemble members that the frequency of TC-EP days either remains about the same or increases markedly in the later period. The enhanced influence from TCs to the NEUS extreme precipitation is attributable both to the increased number of TCs near the NEUS region (Figure 5b) and the strengthened intensity of precipitation over the NEUS related to TCs (Figure 5e). In contrast to the robust change of TC-EP days in the model, SPEAR_HI simulates a large ensemble spread of the change in ET-EP days (Figure 4e): the ratio of frequency between the two periods ranges from 0.79 to 3.50, suggesting substantial internal variability. The large internal variability is also reflected in the ET frequency near the NEUS region: SPEAR_HI ensemble members do not agree on the sign of the change in ET frequency (Figure 5c). Thus, in SPEAR_HI, the increased extreme precipitation over the NEUS in the fall season is dominantly influenced by TCs near the NEUS region in the historical period.

The frequency of intense precipitation on synoptic scale across the NEUS region, namely EP days in this study, has significantly increased since circa the 1990s. The trend is primarily attributed to the enhanced influences from ETs in observations. The observed ET-EP days are twice frequent in 1990–2020 compared to in 1959–1989. In SPEAR_HI, however, the dominant contributor comes from TCs; while the simulated ET-EP days show no significant change in the later period.

To address the discrepancy concerning the contribution of ETs to the NEUS extreme precipitation between the observational and SPEAR_HI results, we next investigate the performance of SPEAR_HI in simulating the frequency of TC-related events, with a particular focus on ETs. Figure 6 presents the track density of TCs that undergo extratropical transition process (upper panels; ET cases) versus TCs that do not undergo extratropical transition process (lower panels; non-ET cases) in September to November from 1959 to 2020 for both JRA-55 and SPEAR_HI. These track density maps consist of the entire life cycle of each cyclone, including the ET as well as TC phases. Comparing between JRA-55 and SPEAR_HI, SPEAR_HI underestimates the frequency over the Gulf of Mexico and overestimates the frequency over the central tropical North Atlantic, in both ET cases and non-ET cases. The overall distributions, nevertheless, show a good agreement between SPEAR_HI and JRA-55, including the recurving feature, the distribution along the East Coast of North America and the poleward latitude to which these cyclones extend. Also, the comparable frequency and spatial distribution of ET-TCs and non-ET-TCs between SPEAR_HI and JRA-55 suggest that the model is proficient to simulate extratropical transition process associated with these TCs. The discrepancy in the contributions of ETs versus TCs to the NEUS extreme precipitation may be related to the location where a TC undergoes extratropical transition process. TCs in SPEAR_HI may experience the transition process "later" in their trajectory compared to what occurs in observations. In this case, in SPEAR_HI, when a cyclone approaches the NEUS region, it is more likely to still be classified as a TC, leading to more extreme precipitation attributed to TCs. Conversely, in observations, the

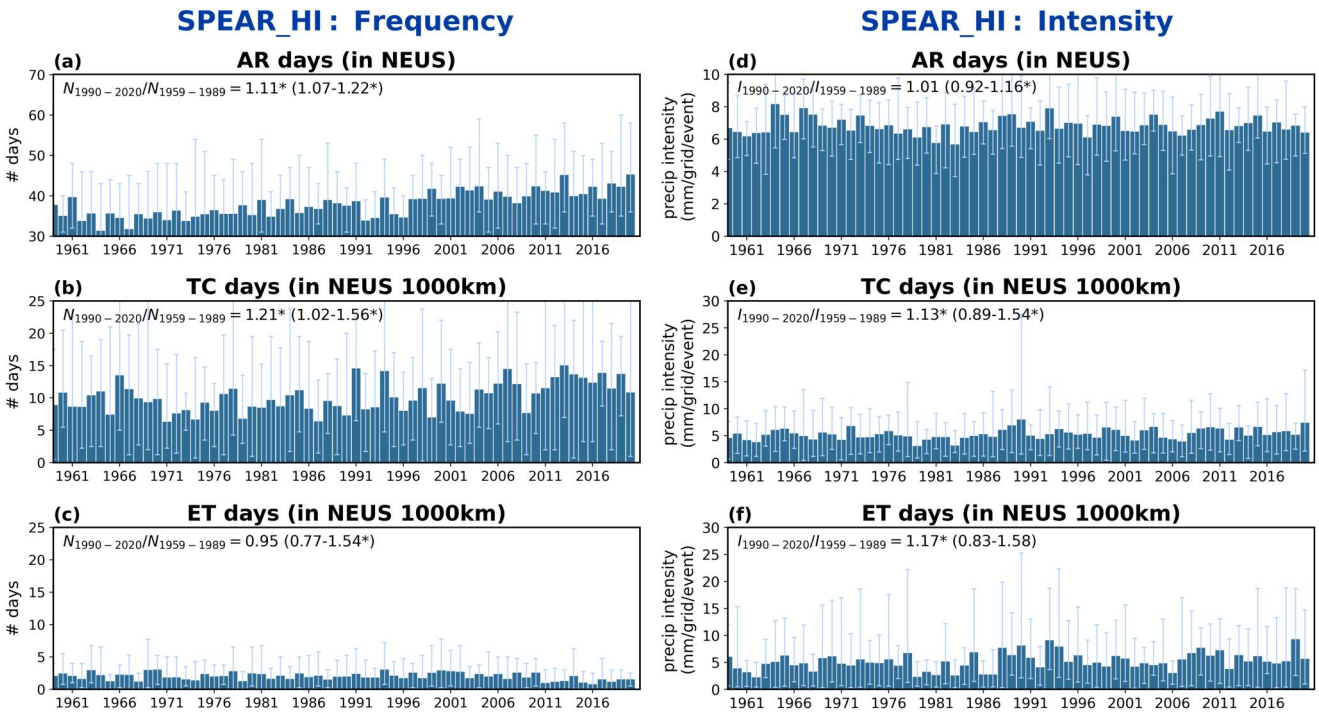

Figure 5. Same as Figure 3, but for SPEAR_HI ensemble simulations. Bars are the ensemble mean of SPEAR_HI. Thin lines indicate the spread across the 10 ensemble members. The ratio numbers in the parentheses are the range of the ratios from each ensemble member.

cyclone is more likely to have already transitioned into an extratropical cyclone when it approaches the NEUS. Details about extratropical transition process in SPEAR_HI are beyond the scope of this work and will be addressed in the future. In general, SPEAR_HI demonstrates its capability to capture TC-related events in vicinity to the NEUS region, causing extreme precipitation over the region.

SPEAR_HI has shown strong performance in simulating the frequency and variability of extreme precipitation over the NEUS in the present climate. Further, SPEAR_HI can reasonably simulate the relative contributions of ARs and TC-related events to the NEUS extreme precipitation. As extreme precipitation over the NEUS is expected to become more frequent due to anthropogenic warming (e.g., DeGaetano & Castellano, 2017; Hayhoe et al., 2007; Jong et al., 2023; Nazarian et al., 2022; Ning et al., 2015; Picard et al., 2023), we next use SPEAR_HI to evaluate how the contributions of ARs and TC-related events to the NEUS extreme precipitation will change in response to anthropogenic warming.

3.3. Future Projections From SPEAR_HI

Under the SSP5-8.5 simulations, EP days are projected to nearly double by the end of the 21st century, based upon the historical climatology from 1959 to 2020 (Figure 7a). The annual averaged EP days in 2091–2100 is about 6.6 days, compared to 3.9 days in 2011–2020. In Jong et al. (2023), they used the same model with the same SSP5-8.5 simulations, showing that the frequency of extreme precipitation, considering all the grid points in the NEUS region based upon the 99th percentile of the 1951–2020 climatology, is projected to become 2.4% by 2100. The results here align with this trend, even though we use the synoptic-scale EP days in this work. In the future projections, the majority of EP days will continue to be predominantly related to either ARs and/or TC-related events (87.6% in total; Table 3, fourth column), although the contribution from ARs will increase: about two-thirds of the EP days will be connected to pure ARs, absent any TC-related events in proximity. This contrasts with the period from 1959 to 2020, during which only about 55.5% of EP days are associated with pure ARs.

The growing relative contribution of pure ARs to extreme precipitation is connected to the projected increase in pure AR-EP days over the NEUS: the total number of pure AR-EP days in 2041–2100 would double when compared to the number in 1961–2020 (Figure 7b). The projected change in pure AR-EP days can be directly attributed to the increase in ARs frequency, which may depend on the AR detection algorithm used. In this study,

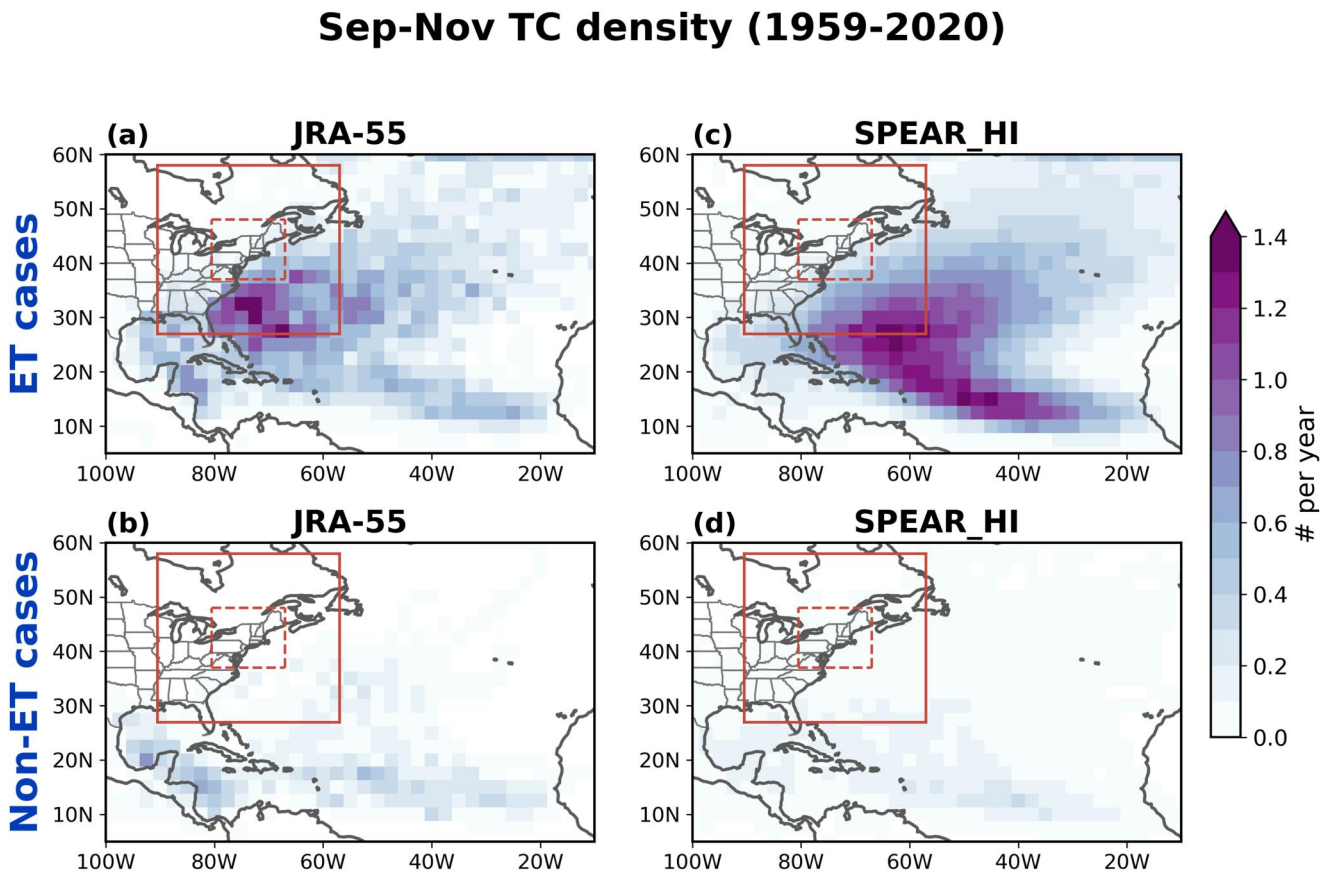

Figure 6. TC density showing the annual averaged frequency of TC in each 2.5° × 2.5° grid box in September–November during the 1959 to 2020 period for (top) ET cases, that is, TCs that experience extratropical transition process and (bottom) non-ET cases, that is, TCs that do not experience extratropical transition process from (left) JRA-55 and (right) SPEAR_HI ensemble mean. Red dashed line boxes indicate the region of the NEUS used in this study. Red solid line boxes indicate the area of 1,000 km from the NEUS.

we employ the AR detection algorithm that uses a fixed IVT threshold based on the 1959–2020 climatology (Mundhenk et al., 2016). Under this approach, the projected change in the AR frequency in the future climate is dominated by the heightened atmospheric moisture content. The number of ARs days over the NEUS region is thereby projected to increase as atmospheric moisture increases with warming climate, leading to more frequent pure AR-EP days. It is worth noting that alternative AR detection algorithms, such as Tempest (Ullrich & Zarzycki, 2017), which uses time-dependent IVT thresholds, have been employed in previous studies. These alternative methods have highlighted that changes in AR frequency can be predominantly influenced by a meridional shift in storm tracks. Nonetheless, the overarching trend of ARs over the NEUS is not affected by the algorithm, both methods show increasing ARs frequency over the NEUS (O'Brien et al., 2022; Tseng et al., 2022; Zhao, 2020). Although the degree of increase in ARs frequency can be affected by whether the algorithm uses a stationary or a time-dependent IVT threshold, we decide to use a stationary IVT threshold based upon the historical climatology. The choice is motivated by the fact that most of the infrastructure has been built upon the historical climatology and this approach can give us a better sense of how extreme precipitation associated with ARs will change compared to the current climate.

TC-related-EP days are also projected to rise, even though the relative contribution of pure ARs to EP days will dominate. The decline in the relative contribution of TC-related events to EP days (Table 3, fourth column) can be attributed to both the increase in the occurrence of ARs and the decrease in TC numbers in the North Atlantic under the SSP5-8.5 simulations. Consistent with the majority of GCMs results (e.g., reviews by Knutson et al., 2020; Sobel et al., 2021), SPEAR_HI projects a decrease in basin-total TC numbers over the North Atlantic in a warming climate: the total number of TCs in the North Atlantic for the period 2041–2100 is projected to be only 60% of the number in 1961–2020 (Figure 8a). Intriguingly, despite the marked decrease in the projected

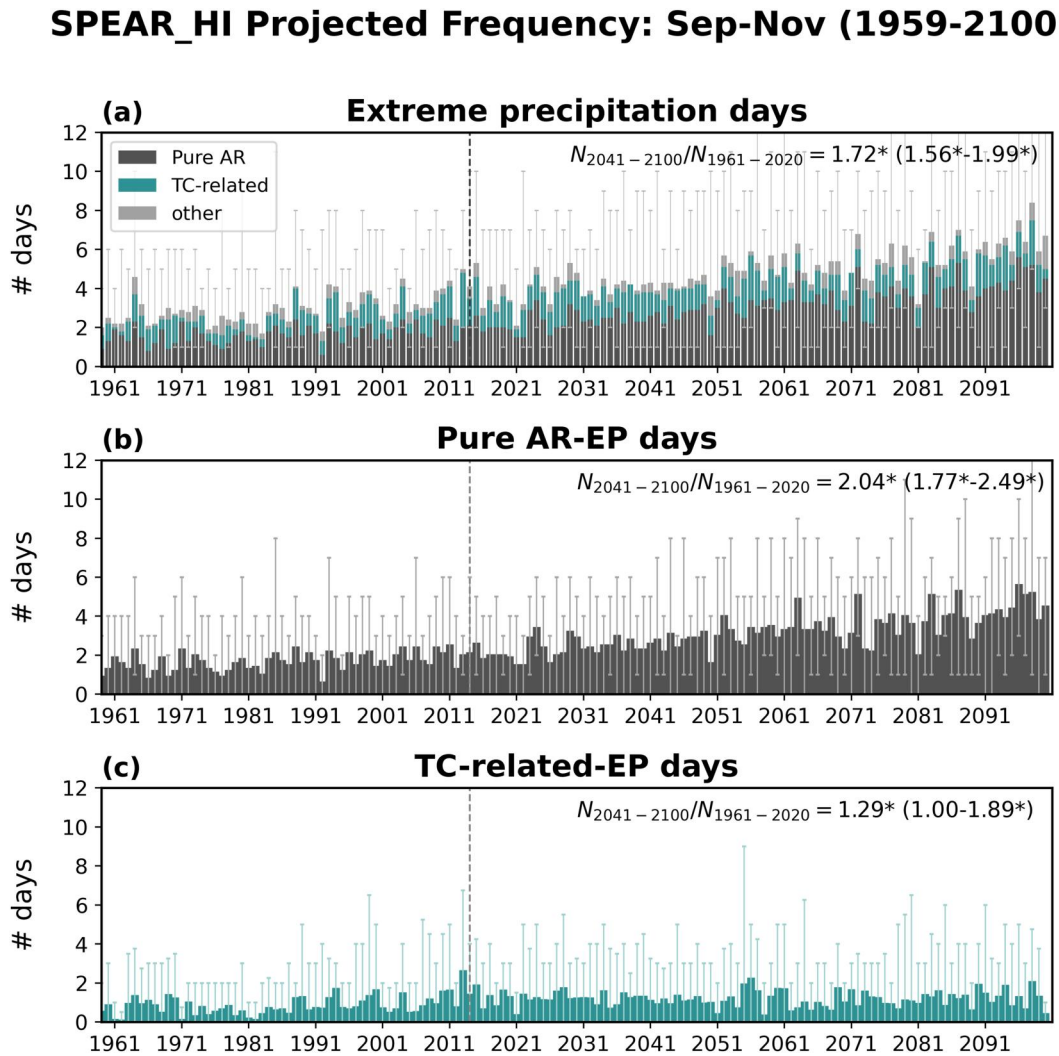

Figure 7. Extreme precipitation (EP) days from SPEAR_HI historical (1959–2014) and SSP5-8.5 (2015–2100) simulations. (a) Time-series for the number of EP days over the NEUS in September–November in each year. The NEUS EP days are further categorized based upon the accompanied synoptic-scale meteorological factors: EP days accompanied by (b) ARs only (pure AR-EP days); (c) TC-related events (TCs or/and ETs; TC-related-EP days). Bars are the ensemble mean of SPEAR_HI. Thin lines indicate the spread of the ensemble members. The numbers in each panel are the ratios between the total numbers of days in 2041–2100 versus the numbers in 1961–2020. Asterisks indicate the differences between the two periods are statistically significant at the 95% confidence level. The vertical black dashed lines indicate the year of 2014, the onset of the SSP5-8.5 projection simulations.

basin-total TC numbers, TC-related-EP days over the NEUS are projected to increase significantly by about 30% in 2041–2100 compared to in 1961–2020 (Figure 7c). Several potential factors may contribute to this distinction: increasing interaction between TCs and ARs, enhancing TC intensity, strengthening TC-related precipitation intensity, and change in TC tracks.

The projected increasing TC-related-EP days may be partially attributed to the greater frequency of ARs coexisting in the NEUS region. As aforementioned, the presence of ARs in the NEUS during a TC-related event is conducive to extreme precipitation over the NEUS compared to a TC-related event occurring alone. With ARs projected to become more frequent in the future, each TC-related event will be more likely to interact with extratropical ARs, bringing more extreme precipitation to the NEUS. In the SPEAR_HI projections, TC-related-EP days with no ARs in the NEUS region shows no change in between 2041–2100 and 1961–2020. In contrast, TC-related-EP days with concurrent ARs in the NEUS are expected to increase largely (Table 2).

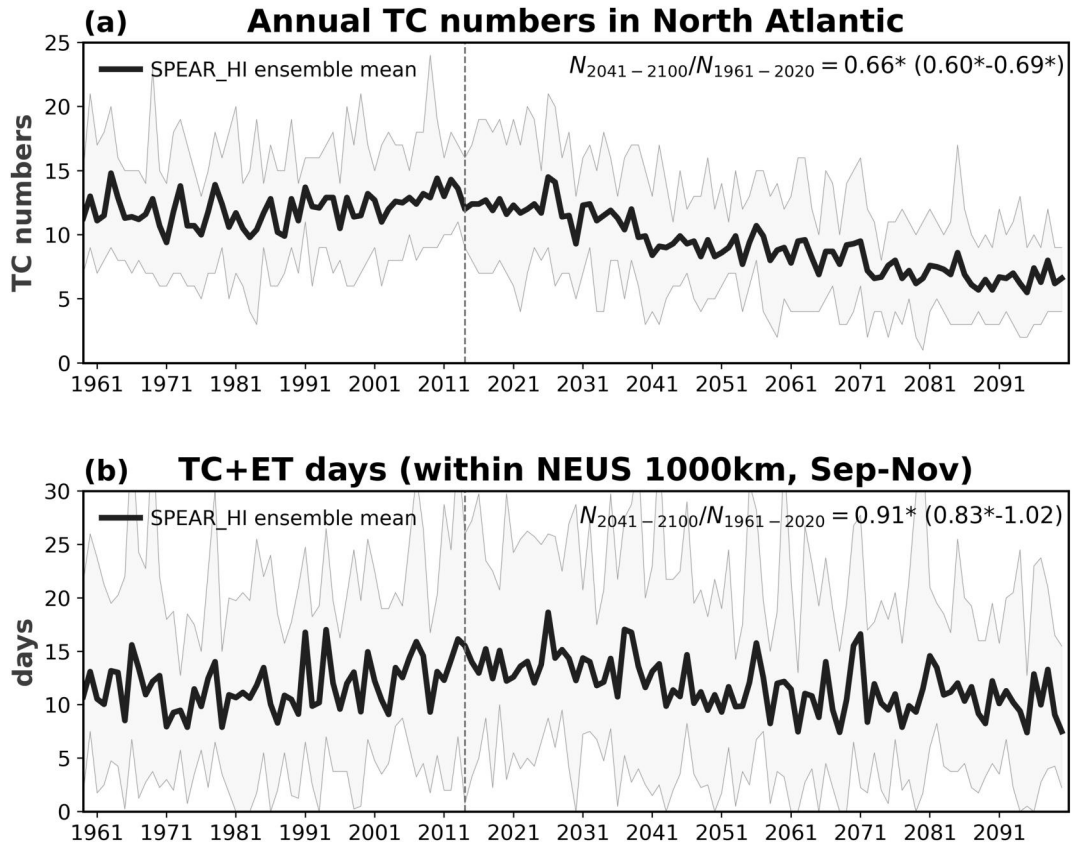

Figure 8. Time-series for SPEAR_HI historical (1959–2014) and SSP5-8.5 (2015–2100) simulations: (a) annual TC numbers in the North Atlantic. The number on the upper right is the ratio of the total TC numbers in 2041–2100 versus the numbers in 1961–2020. (b) The numbers of days that the NEUS and its vicinity experience TCs or/and ETs in September–November each year. The number on the upper right is the ratio of the total days in 2041–2100 versus the numbers in 1961–2020. Asterisks indicate the differences between the two periods are statistically significant at the 95% confidence level. The solid thick black lines are the SPEAR_HI ensemble mean. The gray shaded areas encompass the spread of ensemble members. The vertical black dashed lines indicate the year of 2014, the onset of the SSP5-8.5 projection simulations.

Although TC number is projected to decrease, TC intensity is projected to strengthen in a warming climate. Studies using dynamical models with horizontal resolution of 60 km or finer have agreed on a projected strengthening average maximum TC intensity (e.g., Knutson et al., 2020; Murakami & Sugi, 2010; Patricola & Wehner, 2018). We also examine the change in maximum TC intensity in the SPEAR_HI projections. Figure 9 illustrates the probability density function of averaged lifetime maximum surface wind speed and minimum SLP of TCs in the North Atlantic in each year from all the ensemble members. The distributions of both maximum surface wind speed and minimum SLP of TCs in 2041–2100 are statistically significantly wider than those in 1961–2020. This suggests that, in the future projections, a TC will have higher probability of becoming stronger compared to the current climate. Such intensification of TCs, including the likelihood of major hurricanes, can potentially elevate the risk, including extreme precipitation over densely populated areas such as the NEUS region.

The intensification of near-storm TC precipitation in a warming climate stands as one of the confidently projected changes among various TC activity metrics, based on many previous studies, over both ocean and land area (e.g., Knutson et al., 2020; Liu et al., 2018; Stansfield, Reed, & Zarzycki, 2020; Huang et al., 2021; and references therein). Here, we check the composite of daily precipitation anomalies over the NEUS when there is a TC-related event occurring within 1,000 km from the NEUS in the SPEAR_HI SSP5-8.5 simulations (Figure 10a). The projected precipitation anomalies composite for 2041–2100 are statistically significantly wetter than the composite for 1961–2020 across almost the entire NEUS region. On the other hand, the numbers of precipitation days when there are TC-related events within 1,000 km from the NEUS region are projected to decrease (Figure 10b).

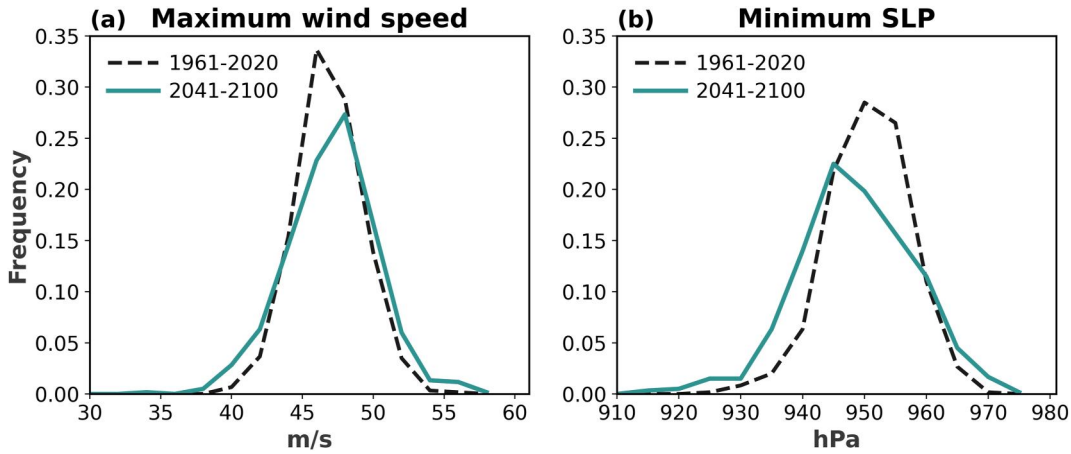

Figure 9. (a) Probability density function of TC lifetime maximum surface wind speed averaged annually per each ensemble member for the 2041–2100 period (green solid line) versus 1961–2020 (black dashed line) in the North Atlantic in SPEAR_HI. (b) Same as (a), but for the TC lifetime minimum SLP.

These results suggest that, even though the NEUS will experience less TC-related days in the future, precipitation rate of each TC-related event will intensify, contributing partially to the increasing TC-related-EP days in the future.

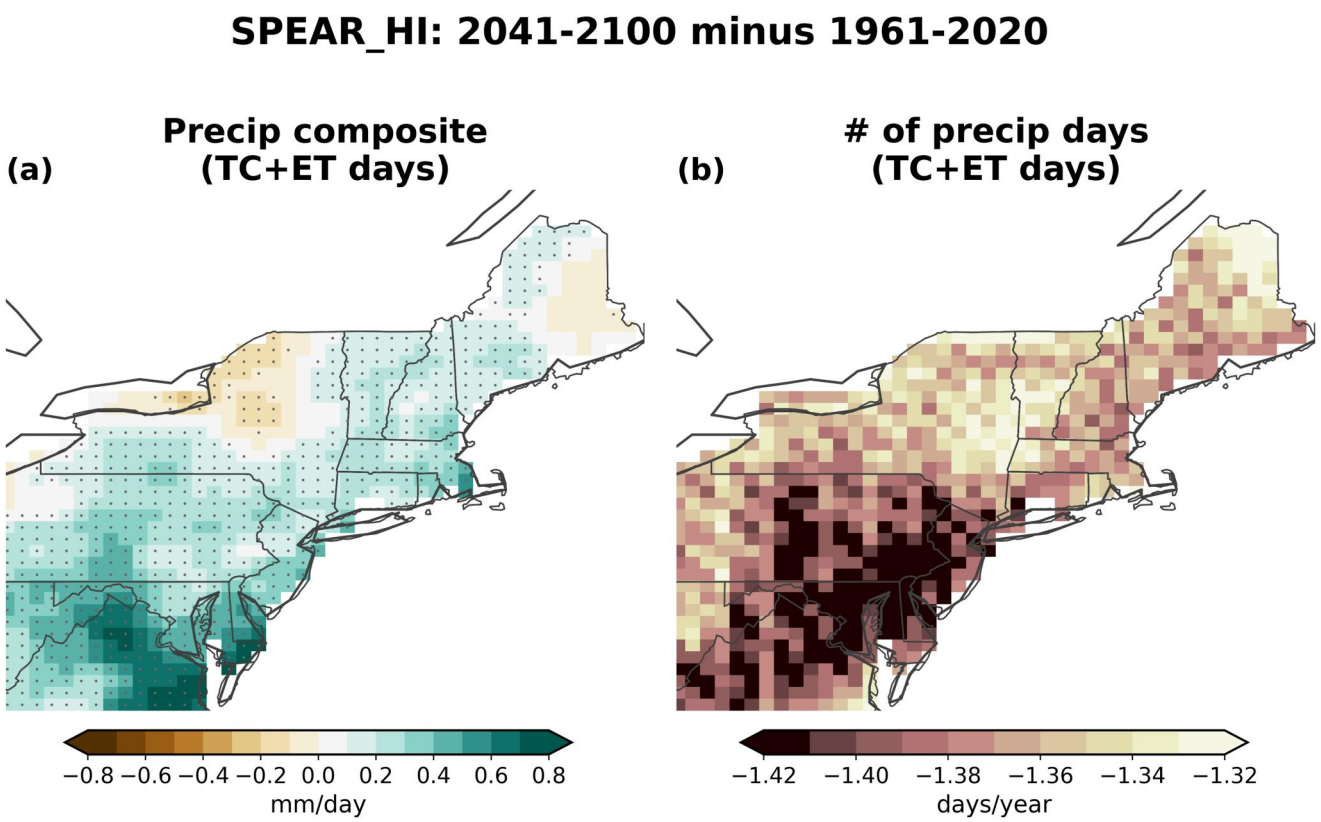

Figure 10. The composites of (a) average precipitation during TC-related days of the NEUS (i.e., there are TCs or/and ETs within 1,000 km from the NEUS region) and (b) the average numbers of precipitation days when there are TCs or/and ETs within 1,000 km from the NEUS region each year. The maps show the composites in 2041–2100 from the SPEAR_HI SSP5-8.5 simulations minus the composites in 1961–2020 from the SPEAR_HI historical simulations. The dots denote the differences between the two periods are statistically significant at the 95% confidence level.

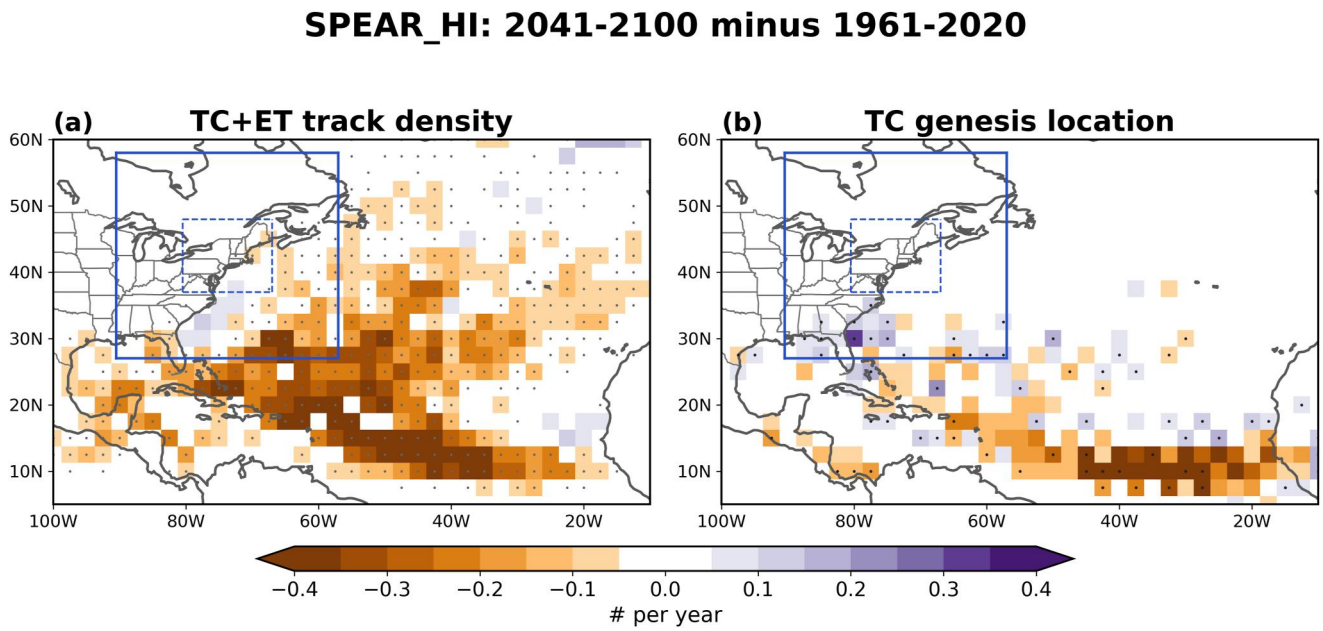

Figure 11. (a) Projected change in the annual September-November frequency of TC-related events (TCs plus ETs) in the SPEAR_HI historical and SSP5-8.5 simulations. The map shows the track density in 2041–2100 minus the track density in 1961–2020. (b) Spatial distribution of projected change in the annual September–November frequency of TC genesis in SPEAR_HI. The map shows the frequency of TC genesis location in 2041–2100 minus the frequency in 1961–2020. The dots denote the differences between the two periods are statistically significant at the 95% confidence level. Blue dashed line boxes indicate the region of the NEUS used in this study. Blue solid line boxes indicate the area of 1,000 km from the NEUS.

The number of days that the NEUS and its vicinity experience TC-related events is projected to decrease. The decreasing rate, however, is much slower than the decreasing rate of TC basin-total numbers (Figure 8). The total days that the NEUS experiences TC-related events in 2041–2100 is about 90% of the number in 1961–2020 (Figure 8b). The discrepancy in the decreasing rates could be related to changes in TC tracks. Figure 11a displays the differences in TC density over the North Atlantic between 2041–2100 and 1961–2020. The TC number is projected to decrease statistically significantly in SPEAR_HI almost everywhere in the North Atlantic, except the region along the east coast of the US. The projected change in the TC number near the East Coast shows no significant change. These spatial varied changes in the TC density imply that TC tracks would shift westward, closer to the US East Coast in a warming climate. The westward shift in the TC tracks can enhance TCs' impacts on the coastal region, even though the TC number would decrease. The shift in the TC tracks might be partially related to the shift in the TC genesis location (Figure 11b): although the model projects marked decline in genesis frequency in the tropical Atlantic, the genesis frequency near the coastal southern US is projected to increase.

In summary, in a future warming climate, both AR-related and TC-related extreme precipitation over the NEUS are projected to increase, even though the numbers of TC in the North Atlantic are projected to decrease in the 25-km GFDL-SPEAR SSP5-8.5 simulations. Factors such as increasing interaction between TCs and ARs, enhancing TC intensity, strengthening TC-related precipitation, and/or westward shift in TC tracks may offset the influence of declining TC numbers in the model projections, leading to more frequent TC-related extreme precipitation over the NEUS.

4. Conclusion and Discussion

In this study, we examine the changes in synoptic-scale contributions to extreme precipitation trends over the NEUS in the fall season in both the historical period and future projections using a high-resolution (25 km atm) model (GFDL SPEAR_HI). We categorize September to November extreme precipitation (EP) days based on daily cumulative precipitation over the NEUS into weather types: EP days accompanied with tropical cyclone-related events (TC-related-EP days), EP days accompanied with atmospheric rivers (ARs) only (pure AR-EP days), and EP days accompanied with neither TC-related nor ARs event (other).

In observations, the majority of EP days are AR days and/or TC-related days. Specifically, approximately 27% of the EP days are linked to TC-related events, while 60% of the EP days are solely attributed to AR events for the 1959 to 2020 period. The primary contribution to the increasing EP days is caused by TC-related events, especially the influence from extratropical transitions (ETs). The EP days associated with ETs have occurred twice as frequently during the 1990 to 2020 period compared to the preceding 1959 to 1989 period. The number of pure AR-EP days, on the other hand, exhibits no statistically significant trend from 1959 to 2020. We apply the same analysis to the SPEAR_HI historical simulations. Similar to observations, the rising EP days are mainly attributed to TC-related events, with a smaller influence from pure AR events. Interestingly, the increasing number of TC-related-EP days in SPEAR_HI is dominated by TCs, whereas the number of EP days associated with ETs changes very little from 1959 to 2020. Despite the discrepancy, SPEAR_HI faithfully simulates the relative contributions of ARs and TC-related events to extreme precipitation over the NEUS similar to observations. Also, SPEAR_HI captures the contribution of TC-related events to the extreme precipitation trend over the region for the historical period.

In the SPEAR_HI SSP5-8.5 projections, when employing the same criteria based on the climatology of 1959–2020, both AR-related and TC-related EP days over the NEUS are projected to increase. The increase in pure AR-EP days is projected to outpace the increase in TC-related-EP days. This projected rise in pure AR-EP days can be directly attributed to the heightened frequency of AR events, a consequence of the increase in atmospheric moisture in response to the warming climate. On the other hand, the slower increase in TC-related-EP days is restrained by the projected decrease in TC number over the North Atlantic in a warming climate. Nevertheless, in spite of the projected decrease in the North Atlantic TCs, TC-related-EP days are projected to surge by about 50% by the late 21st century. The effect of decreasing TC number is overpowered via several factors. These include intensification of TCs, strengthened TC-related precipitation, shifts in TC tracks and genesis locations, and rising interaction between TCs and AR events.

Changes in the relative contribution of ARs or TC-related events to extreme precipitation play a significant role in shaping the spatial distribution of precipitation. Precipitation caused by midlatitude systems such as ARs and ETs tends to cover a broader area across the NEUS, including inland locations (e.g., Evans et al., 2017). Conversely, precipitation caused by TCs tends to be more localized and closer to the coastal regions with stronger intensity (Figures S2 and S3 in Supporting Information S1). These differences in the spatial patterns of extreme precipitation during different weather types have profound implications for flood prevention and mitigation strategies.

Compared with observations, SPEAR_HI exhibits a discrepancy in simulating trends in EP days associated with TCs compared to those associated with ETs. In observations, the increasing trend of EP days is primarily attributed to ETs, while in SPEAR_HI, influences from TCs dominate the increasing trend of EP days. One possible explanation for this disparity is that in SPEAR_HI, TCs may undergo extratropical transition process later than they do in observations. SPEAR_HI can still effectively replicate extreme precipitation pattern and frequency caused by TC-related events in proximity to the NEUS region when we aggregate TCs and ETs as TC-related events. However, since the precipitation spatial patterns caused by TCs and ETs differ substantially (Figures S2 and S3 in Supporting Information S1), caution should be taken when utilizing the model projection to address future extreme precipitation associated with TC-related events.

The discrepancy in simulating the latitude and timing at which TCs undergo extratropical transition may lead to other potential impacts besides the spatial pattern of precipitation across the NEUS. For example, transitioning cyclones can alter the large-scale circulation such as exciting downstream Rossby waves and modulating downstream weather patterns (e.g., Evans et al., 2017; Michaelis & Lackmann, 2019). The potential consequences of this discrepancy in ETs on downstream hydroclimate extreme simulation in SPEAR_HI, as well as the underlying reasons for this discrepancy are subjects for future work.

Another caveat of this study is that we have relied solely on one climate model. Our choice is limited by the availability of fully coupled climate models with higher horizontal resolution that permit the more realistic representations of the spectrum of TC intensities and multiple ensemble members. Previous research has indicated that larger ensembles (>10 members) are essential to assess the multidecadal variability of very extreme precipitation events in the NEUS (Jong et al., 2023). Despite this limitation, several key findings in our study align with previous studies. For instance, other studies using CMIP5/6 models, based on either stationary or time-dependent IVT thresholds, have projected increases in the frequency of ARs over Northeastern North America (e.g., O'Brien et al., 2022). Additionally, AR-related precipitation has also been shown to intensify in response to

a warming climate (e.g., Nellikkattil et al., 2023). Both of these are consistent with our finding that pure AR-EP days will become more frequent in the future.

Larger uncertainties in our results arise from the projections regarding TCs. The question whether the number of TCs over the North Atlantic will decrease in a future warming climate remains highly uncertain (as discussed in Knutson et al., 2020; Sobel et al., 2021). On the contrary, there is more robust evidence supporting increases in TC intensity and the intensity of TC-related precipitation (e.g., Kitoh & Endo, 2019; Knutson et al., 2020; Liu et al., 2018; Patricola & Wehner, 2018; Stansfield, Reed, & Zarzycki, 2020; Wright et al., 2015). Other aspects of TC projections, such as shifts in TC tracks and genesis locations closer to the US East Coast, introduce further uncertainties as based on just one climate model projection. Also, TC genesis locations and tracks in SPEAR_HI have presented some inconsistencies compared with observations. Nonetheless, our study underscores that the changing contribution of TCs to regional extreme precipitation along the US East Coast in the future warming climate is subject to a wide array of factors. Even if the TC number declines in the future, the frequency of extreme precipitation events associated with TCs may still rise.

Conflict of Interest

The authors declare no conflicts of interest relevant to this study.

Data Availability Statement

SPEAR_HI is described in Delworth et al. (2020), Jong et al. (2023), and at https://www.gfdl.noaa.gov/spear/ (GFDL SPEAR, 2023). The CPC Unified Gauge-Based gridded daily precipitation data are available on the IRI/LDEO Climate Data Library (IRI/LDEO Climate Data Library, 2023). The JRA-55 reanalysis data can be accessed from the NCAR Research Data Archive (NCAR Research Data Archive, 2023). All data for this study is available at https://doi.org/10.5281/zenodo.10346929 (Jong et al., 2024).

Acknowledgments
We thank Drs. Tsung-Lin Hsieh and Akshaya Nikumbh for constructive comments on an internal review of the manuscript. We appreciate Drs. Kai-Chih Tseng, Zachary Labe, Chia-Ying Lee, Jorge Garcia-Franco, Alexander Baker, and Xiangbo Feng for their discussions and feedback on various aspects of this research. We also acknowledge two anonymous reviewers for their constructive comments. Bor-Ting Jong received award NA18OAR4320123 from the National Oceanic and Atmospheric Administration, U.S. Department of Commerce. We acknowledge GFDL resources made available for this research. The statements, findings, conclusions, and recommendations are those of the author(s) and do not necessarily reflect the views of the National Oceanic and Atmospheric Administration, or the U.S. Department of Commerce.

References

Adcroft, A., Anderson, W., Balaji, V., Blanton, C., Bushuk, M., Dufour, C. O., et al. (2019). The GFDL global ocean and sea ice model OM4.0: Model description and simulation features. *Journal of Advances in Modeling Earth Systems*, *11*(10), 3167–3211. https://doi.org/10.1029/2019ms001726

Agel, L., Barlow, M., Feldstein, S. B., & Gutowski, W. J. (2018). Identification of large-scale meteorological patterns associated with extreme precipitation in the US northeast. *Climate Dynamics*, *50*(5–6), 1819–1839. https://doi.org/10.1007/s00382-017-3724-8

Agel, L., Barlow, M., Qian, J.-H., Colby, F., Douglas, E., & Eichler, T. (2015). Climatology of daily precipitation and extreme precipitation events in the Northeast United States. *Journal of Hydrometeorology*, *16*(6), 2537–2557. https://doi.org/10.1175/jhm-d-14-0147.1

Akinsanola, A. A., J, K. G., Pendergrass, A. G., M, W. M. H. W., & Reed, K. A. (2020). Seasonal representation of extreme precipitation indices over the United States in CMIP6 present-day simulations. *Environmental Research Letters*, *15*(9), 094003. https://doi.org/10.1088/1748-9326/ab92c1

Anderson, B. T., Gianotti, D. J., & Salvucci, G. D. (2015). Detectability of historical trends in station-based precipitation characteristics over the continental United States. *Journal of Geophysical Research: Atmospheres*, *120*(10), 4842–4859. https://doi.org/10.1002/2014jd022960

Baker, A. J., Roberts, M. J., Vidale, P. L., Hodges, K. I., Seddon, J., Vannière, B., et al. (2022). Extratropical transition of tropical cyclones in a multiresolution ensemble of atmosphere-only and fully coupled global climate models. *Journal of Climate*, *35*(16), 5283–5306. https://doi.org/10.1175/jcli-d-21-0801.1

Barlow, M. (2011). Influence of hurricane-related activity on North American extreme precipitation. *Geophysical Research Letters*, *38*(4), L04705. https://doi.org/10.1029/2010gl046258

Barlow, M., Gutowski, W. J., Gyakum, J. R., Katz, R. W., Lim, Y.-K., Schumacher, R. S., et al. (2019). North American extreme precipitation events and related large-scale meteorological patterns: A review of statistical methods, dynamics, modeling, and trends. *Climate Dynamics*, *53*(11), 6835–6875. https://doi.org/10.1007/s00382-019-04958-z

Bhatia, K., Vecchi, G., Murakami, H., Underwood, S., & Kossin, J. (2018). Projected response of tropical cyclone intensity and intensification in a global climate model. *Journal of Climate*, *31*(20), 8281–8303. https://doi.org/10.1175/jcli-d-17-0898.1

Bieli, M., Camargo, S. J., Sobel, A. H., Evans, J. L., & Hall, T. (2019). A global climatology of extratropical transition. Part I: Characteristics across basins. *Journal of Climate*, *32*(12), 3557–3582. https://doi.org/10.1175/jcli-d-17-0518.1

Bieli, M., Sobel, A. H., Camargo, S. J., Murakami, H., & Vecchi, G. A. (2020). Application of the cyclone phase space to extratropical transition in a global climate model. *Journal of Advances in Modeling Earth Systems*, *12*(4), e2019MS001878. https://doi.org/10.1029/2019ms001878

Brown, P. J., Bradley, R. S., & Keimig, F. T. (2010). Changes in extreme climate indices for the northeastern United States, 1870–2005. *Journal of Climate*, *23*(24), 6555–6572. https://doi.org/10.1175/2010jcli3363.1

Burgess, M. G., Ritchie, J., Shapland, J., & Pielke, R. (2021). IPCC baseline scenarios have over-projected CO_2 emissions and economic growth. *Environmental Research Letters*, *16*(1), 014016. https://doi.org/10.1088/1748-9326/abcdd2

Camargo, S. J., & Wing, A. A. (2016). Tropical cyclones in climate models. *Wiley Interdisciplinary Reviews: Climate Change*, *7*(2), 211–237. https://doi.org/10.1002/wcc.373

Chen, M., Shi, W., Xie, P., Silva, V. B. S., Kousky, V. E., Higgins, R. W., & Janowiak, J. E. (2008). Assessing objective techniques for gauge-based analyses of global daily precipitation. *Journal of Geophysical Research - Atmosphere*, *113*(D4), D04110. https://doi.org/10.1029/2007jd009132

Crossett, C. C., Dupigny-Giroux, L.-A. L., Kunkel, K. E., Betts, A. K., & Bomblies, A. (2023). Synoptic typing of multiduration, heavy precipitation records in the northeastern United States: 1895–2017. *Journal of Applied Meteorology and Climatology*, *62*(6), 721–736. https://doi.org/10.1175/jamc-d-22-0091.1

DeGaetano, A. T. (2009). Time-dependent changes in extreme-precipitation return-period amounts in the continental United States. *Journal of Applied Meteorology and Climatology*, *48*(10), 2086–2099. https://doi.org/10.1175/2009jamc2179.1

DeGaetano, A. T., & Castellano, C. M. (2017). Future projections of extreme precipitation intensity-duration-frequency curves for climate adaptation planning in New York State. *Climate Services*, *5*, 23–35. https://doi.org/10.1016/j.cliser.2017.03.003

DeGaetano, A. T., Moores, G., & Favata, T. (2020). Temporal changes in the areal coverage of daily extreme precipitation in the northeastern United States using high-resolution gridded data. *Journal of Applied Meteorology and Climatology*, *59*(3), 551–565. https://doi.org/10.1175/jamc-d-19-0210.1

Delworth, T. L., Cooke, W. F., Adcroft, A., Bushuk, M., Chen, J., Dunne, K. A., et al. (2020). SPEAR: The next generation GFDL modeling system for seasonal to multidecadal prediction and projection. *Journal of Advances in Modeling Earth Systems*, *12*(3), e2019MS00189. https://doi.org/10.1029/2019ms001895

Demory, M.-E., Vidale, P. L., Roberts, M. J., Berrisford, P., Strachan, J., Schiemann, R., & Mizielinski, M. S. (2014). The role of horizontal resolution in simulating drivers of the global hydrological cycle. *Climate Dynamics*, *42*(7–8), 2201–2225. https://doi.org/10.1007/s00382-013-1924-4

Easterling, Kunkel, D. R., Arnold, K. E., Knutson, J. R., LeGrande, T., Leung, A. N., et al. (2017). Precipitation change in the United States. In D. J. Wuebbles, D. W. Fahey, K. A. Hibbard, D. J. Dokken, B. C. Stewart, & T. K. Maycock (Eds.), *Climate science special report: Fourth national climate assessment* (Vol. I, pp. 207–230). U.S. Global Change Research Program. https://doi.org/10.7930/j0h993cc

Emanuel, K. A. (2013). Downscaling CMIP5 climate models shows increased tropical cyclone activity over the 21st century. *Proceedings of the National Academy of Sciences*, *110*(30), 12219–12224. https://doi.org/10.1073/pnas.1301293110

Emanuel, K. A. (2021). Response of global tropical cyclone activity to increasing CO_2: Results from downscaling CMIP6 models. *Journal of Climate*, *34*(1), 57–70. https://doi.org/10.1175/jcli-d-20-0367.1

Espinoza, V., Waliser, D. E., Guan, B., Lavers, D. A., & Ralph, F. M. (2018). Global analysis of climate change projection effects on atmospheric rivers. *Geophysical Research Letters*, *45*(9), 4299–4308. https://doi.org/10.1029/2017gl076968

Evans, C., Wood, K. M., Aberson, S. D., Archambault, H. M., Milrad, S. M., Bosart, L. F., et al. (2017). The extratropical transition of tropical cyclones. Part I: Cyclone evolution and direct impacts. *Monthly Weather Review*, *145*(11), 4317–4344. https://doi.org/10.1175/mwr-d-17-0027.1

Fiorino, M. (2002). Analysis and forecasts of tropical cyclones in the ECMWF 40-year reanalysis (ERA-40). In *Extended abstract of 25th conference on hurricanes and tropical meteorology* (pp. 261–264).

Frei, A., Kunkel, K. E., & Matonse, A. (2015). The seasonal nature of extreme hydrological events in the northeastern United States. *Journal of Hydrometeorology*, *16*(5), 2065–2085. https://doi.org/10.1175/jhm-d-14-0237.1

Galarneau, T. J., Jr., Bosart, L. F., & Schumacher, R. S. (2010). Predecessor rain events ahead of tropical cyclones. *Monthly Weather Review*, *138*(8), 3272–3297. https://doi.org/10.1175/2010mwr3243.1

Garner, A. J., Kopp, R. E., & Horton, B. P. (2021). Evolving tropical cyclone tracks in the North Atlantic in a warming climate. *Earth's Future*, *9*(12). https://doi.org/10.1029/2021ef002326

GFDL SPEAR. (2023). Retrieved from https://www.gfdl.noaa.gov/spear/

Gori, A., Lin, N., Xi, D., & Emanuel, K. (2022). Tropical cyclone climatology change greatly exacerbates US extreme rainfall–surge hazard. *Nature Climate Change*, *12*(2), 171–178. https://doi.org/10.1038/s41558-021-01272-7

Guilbert, J., Betts, A. K., Rizzo, D. M., Beckage, B., & Bomblies, A. (2015). Characterization of increased persistence and intensity of precipitation in the northeastern United States. *Geophysical Research Letters*, *42*(6), 1888–1893. https://doi.org/10.1002/2015gl063124

Hagos, S. M., Leung, L. R., Yoon, J., Lu, J., & Gao, Y. (2016). A projection of changes in landfalling atmospheric river frequency and extreme precipitation over western North America from the Large Ensemble CESM simulations. *Geophysical Research Letters*, *43*(3), 1357–1363. https://doi.org/10.1002/2015gl067392

Hall, T. M., & Kossin, J. P. (2019). Hurricane stalling along the North American coast and implications for rainfall. *npj Climate and Atmospheric Science*, *2*(1), 17. https://doi.org/10.1038/s41612-019-0074-8

Hallam, S., McCarthy, G. D., Feng, X., Josey, S. A., Harris, E., Düsterhus, A., et al. (2023). The relationship between sea surface temperature anomalies, wind and translation speed and North Atlantic tropical cyclone rainfall over ocean and land. *Environmental Research Communications*, *5*(2), 025007. https://doi.org/10.1088/2515-7620/acb31c

Hart, R. E. (2003). A cyclone phase space derived from thermal wind and thermal asymmetry. *Monthly Weather Review*, *131*(4), 585–616. https://doi.org/10.1175/1520-0493(2003)131<0585:acpsdf>2.0.co;2

Hatsushika, H., Tsutsui, J., Fiorino, M., & Onogi, K. (2006). Impact of wind profile retrievals on the analysis of tropical cyclones in the JRA-25 reanalysis. *Journal of the Meteorological Society of Japan. Ser. II*, *84*(5), 891–905. https://doi.org/10.2151/jmsj.84.891

Hausfather, Z., & Peters, G. P. (2020). Emissions—The "business as usual" story is misleading. *Nature*, *577*(7792), 618–620. https://doi.org/10.1038/d41586-020-00177-3

Hayhoe, K., Wake, C. P., Huntington, T. G., Luo, L., Schwartz, M. D., Sheffield, J., et al. (2007). Past and future changes in climate and hydrological indicators in the US Northeast. *Climate Dynamics*, *28*(4), 381–407. https://doi.org/10.1007/s00382-006-0187-8

Held, I. M., Guo, H., Adcroft, A., Dunne, J. P., Horowitz, L. W., Krasting, J., et al. (2019). Structure and performance of GFDL's CM4.0 climate model. *Journal of Advances in Modeling Earth Systems*, *11*(11), 3691–3727. https://doi.org/10.1029/2019ms001829

Henny, L., Thorncroft, C. D., & Bosart, L. F. (2022). Changes in large-scale fall extreme precipitation in the Mid-Atlantic and Northeast United States, 1979–2019. *Journal of Climate*, *35*(20), 3047–3070. https://doi.org/10.1175/jcli-d-21-0953.1

Henny, L., Thorncroft, C. D., & Bosart, L. F. (2023). Changes in seasonal large-scale extreme precipitation in the Mid-Atlantic and Northeast United States, 1979–2019. *Journal of Climate*, *36*(36), 1017–1042. https://doi.org/10.1175/jcli-d-22-0088.1

Hersbach, H., Bell, B., Berrisford, P., Hirahara, S., Horányi, A., Muñoz-Sabater, J., et al. (2020). The ERA5 global reanalysis. *Quarterly Journal of the Royal Meteorological Society*, *146*(730), 1999–2049. https://doi.org/10.1002/qj.3803

Hoerling, M., Eischeid, J., Perlwitz, J., Quan, X.-W., Wolter, K., & Cheng, L. (2016). Characterizing recent trends in U.S. heavy precipitation. *Journal of Climate*, *29*(7), 2313–2332. https://doi.org/10.1175/jcli-d-15-0441.1

Howarth, M. E., Thorncroft, C. D., & Bosart, L. F. (2019). Changes in extreme precipitation in the Northeast United States: 1979–2014. *Journal of Hydrometeorology*, *20*(4), 673–689. https://doi.org/10.1175/jhm-d-18-0155.1

Hsieh, T.-L., Yang, W., Vecchi, G. A., & Zhao, M. (2022). Model spread in the tropical cyclone frequency and seed propensity index across global warming and ENSO-like perturbations. *Geophysical Research Letters*, *49*(7), e2021GL097157. https://doi.org/10.1029/2021gl097157

Hsieh, T.-L., Zhang, B., Yang, W., Vecchi, G. A., Zhao, M., Soden, B. J., & Wang, C. (2023). The influence of large-scale radiation anomalies on tropical cyclone frequency. *Journal of Climate*, *36*(16), 5431–5441. https://doi.org/10.1175/jcli-d-22-0449.1

Hsu, H.-H., & Chen, Y.-T. (2020). Simulation and projection of circulations associated with atmospheric rivers along the North American Northeast Coast. *Journal of Climate*, *33*(13), 5673–5695. https://doi.org/10.1175/jcli-d-19-0104.1

Huang, H., Patricola, C. M., & Collins, W. D. (2021). The influence of ocean coupling on simulated and projected tropical cyclone precipitation in the HighResMIP–PRIMAVERA simulations. *Geophysical Research Letters*, *48*(20), e2021GL094801. https://doi.org/10.1029/2021gl094801

Huang, H., Patricola, C. M., Winter, J. M., Osterberg, E. C., & Mankin, J. S. (2021). Rise in Northeast US extreme precipitation caused by Atlantic variability and climate change. *Weather and Climate Extremes*, *33*, 100351. https://doi.org/10.1016/j.wace.2021.100351

Huang, H., Winter, J. M., & Osterberg, E. C. (2018). Mechanisms of abrupt extreme precipitation change over the northeastern United States. *Journal of Geophysical Research: Atmospheres*, *123*(14), 7179–7192. https://doi.org/10.1029/2017jd028136

Huang, H., Winter, J. M., Osterberg, E. C., Horton, R. M., & Beckage, B. (2017). Total and extreme precipitation changes over the northeastern United States. *Journal of Hydrometeorology*, *18*(6), 1783–1798. https://doi.org/10.1175/jhm-d-16-0195.1

Iles, C. E., Vautard, R., Strachan, J., Joussaume, S., Eggen, B. R., & Hewitt, C. D. (2020). The benefits of increasing resolution in global and regional climate simulations for European climate extremes. *Geoscientific Model Development*, *13*(11), 5583–5607. https://doi.org/10.5194/gmd-13-5583-2020

IRI/LDEO Climate Data Library. (2023). CPC unified gauge-based gridded daily precipitation data [Dataset]. *IRI/LDEO Climate Data Library*. Retrieved from https://iridl.ldeo.columbia.edu/SOURCES/.NOAA/.NCEP/.CPC/.UNIFIED_PRCP/.GAUGE_BASED/.CONUS/

Janssen, E., Wuebbles, D. J., Kunkel, K. E., Olsen, S. C., & Goodman, A. (2014). Observational- and model-based trends and projections of extreme precipitation over the contiguous United States. *Earth's Future*, *2*(2), 99–113. https://doi.org/10.1002/2013ef000185

Jing, R., Lin, N., Emanuel, K., Vecchi, G., & Knutson, T. R. (2021). A comparison of tropical cyclone projections in a high-resolution global climate model and from downscaling by statistical and statistical-deterministic methods. *Journal of Climate*, *34*, 9349–9364. https://doi.org/10.1175/jcli-d-21-0071.1

Jong, B.-T., Delworth, T. L., Cooke, W. F., Tseng, K.-C., & Murakami, H. (2023). Increases in extreme precipitation over the Northeast United States using high-resolution climate model simulations. *npj Climate and Atmospheric Science*, *6*(1), 18. https://doi.org/10.1038/s41612-023-00347-w

Jong, B.-T., Murakami, H., Delworth, T., & Cooke, W. (2024). Northeast US extreme precipitation trends in GFDL SPEAR_HI [Dataset]. *Zenodo*. https://doi.org/10.5281/zenodo.10346929

Jung, C., & Lackmann, G. M. (2019). Extratropical transition of Hurricane Irene (2011) in a changing climate. *Journal of Climate*, *32*(15), 4847–4871. https://doi.org/10.1175/jcli-d-18-0558.1

Jung, C., & Lackmann, G. M. (2021). The response of extratropical transition of tropical cyclones to climate change: Quasi-idealized numerical experiments. *Journal of Climate*, *34*(11), 4361–4381. https://doi.org/10.1175/jcli-d-20-0543.1

Jung, C., & Lackmann, G. M. (2023). Changes in tropical cyclones undergoing extratropical transition in a warming climate: Quasi-idealized numerical experiments of North Atlantic landfalling events. *Geophysical Research Letters*, *50*(8), e2022GL101963. https://doi.org/10.1029/2022gl101963

Kitoh, A., & Endo, H. (2019). Future changes in precipitation extremes associated with tropical cyclones projected by large-ensemble simulations. *Journal of the Meteorological Society of Japan. Series II*, *97*(1), 141–152. https://doi.org/10.2151/jmsj.2019-007

Knutson, T., Camargo, S. J., Chan, J. C. L., Emanuel, K., Ho, C.-H., Kossin, J., et al. (2020). Tropical cyclones and climate change assessment: Part II. Projected response to anthropogenic warming. *Bulletin of the American Meteorological Society*, *101*(3), E303–E322. https://doi.org/10.1175/bams-d-18-0194.1

Knutson, T., Sirutis, J. J., Bender, M. A., Tuleya, R. E., & Schenkel, B. A. (2022). Dynamical downscaling projections of late twenty-first-century U.S. landfalling hurricane activity. *Climatic Change*, *171*(3–4), 28. https://doi.org/10.1007/s10584-022-03346-7

Kobayashi, S., Ota, Y., Harada, Y., Ebita, A., Moriya, M., Onoda, H., et al. (2015). The JRA-55 reanalysis: General specifications and basic characteristics. *Journal of the Meteorological Society of Japan. Ser. II*, *93*(1), 5–48. https://doi.org/10.2151/jmsj.2015-001

Kopparla, P., Fischer, E. M., Hannay, C., & Knutti, R. (2013). Improved simulation of extreme precipitation in a high-resolution atmosphere model. *Geophysical Research Letters*, *40*(21), 5803–5808. https://doi.org/10.1002/2013gl057866

Kunkel, K. E., Easterling, D. R., Kristovich, D. A. R., Gleason, B., Stoecker, L., & Smith, R. (2012). Meteorological causes of the secular variations in observed extreme precipitation events for the conterminous United States. *Journal of Hydrometeorology*, *13*(3), 1131–1141. https://doi.org/10.1175/jhm-d-11-0108.1

Kunkel, K. E., Karl, T. R., Brooks, H., Kossin, J., Lawrimore, J. H., Arndt, D., et al. (2013). Monitoring and understanding trends in extreme storms: State of knowledge. *Bulletin of the American Meteorological Society*, *94*(4), 499–514. https://doi.org/10.1175/bams-d-11-00262.1

Lee, C.-Y., Camargo, S. J., Sobel, A. H., & Tippett, M. K. (2020). Statistical-dynamical downscaling projections of tropical cyclone activity in a warming climate: Two diverging genesis scenarios. *Journal of Climate*, *33*(11), 4815–4834. https://doi.org/10.1175/jcli-d-19-0452.1

Lee, C.-Y., Sobel, A. H., Camargo, S. J., Tippett, M. K., & Yang, Q. (2022). New York State hurricane hazard: History and future projections. *Journal of Applied Meteorology and Climatology*, *61*(6), 613–629. https://doi.org/10.1175/jamc-d-21-0173.1

Lee, C.-Y., Sobel, A. H., Tippett, M. K., Camargo, S. J., Wüest, M., Wehner, M., & Murakami, H. (2023). Climate change signal in Atlantic tropical cyclones today and near future. *Earth's Future*, *11*, e2023EF003539. https://doi.org/10.1029/2023ef003539

Liu, M., & Smith, J. A. (2016). Extreme rainfall from landfalling tropical cyclones in the eastern United States: Hurricane Irene (2011). *Journal of Hydrometeorology*, *17*(11), 2883–2904. https://doi.org/10.1175/jhm-d-16-0072.1

Liu, M., Vecchi, G. A., Smith, J. A., & Murakami, H. (2017). The present-day simulation and twenty-first-century projection of the climatology of extratropical transition in the North Atlantic. *Journal of Climate*, *30*(8), 2739–2756. https://doi.org/10.1175/jcli-d-16-0352.1

Liu, M., Vecchi, G. A., Smith, J. A., & Murakami, H. (2018). Projection of landfalling tropical cyclone rainfall in the eastern United States under anthropogenic warming. *Journal of Climate*, *31*(18), 7269–7286. https://doi.org/10.1175/jcli-d-17-0747.1

Liu, M., Yang, L., Smith, J. A., & Vecchi, G. A. (2020). Response of extreme rainfall for landfalling tropical cyclones undergoing extratropical transition to projected climate change: Hurricane Irene (2011). *Earth's Future*, *8*(3), e2019EF001360. https://doi.org/10.1029/2019ef001360

Lucas-Picher, P., Laprise, R., & Winger, K. (2017). Evidence of added value in North American regional climate model hindcast simulations using ever-increasing horizontal resolutions. *Climate Dynamics*, *48*(7–8), 2611–2633. https://doi.org/10.1007/s00382-016-3227-z

Menne, M. J., Durre, I., Vose, R. S., Gleason, B. E., & Houston, T. G. (2012). An overview of the global historical climatology network-daily database. *Journal of Atmospheric and Oceanic Technology*, *29*(7), 897–910. https://doi.org/10.1175/jtech-d-11-00103.1

Michaelis, A. C., & Lackmann, G. M. (2019). Climatological changes in the extratropical transition of tropical cyclones in high-resolution global simulations. *Journal of Climate*, *32*(24), 8733–8753. https://doi.org/10.1175/jcli-d-19-0259.1

Min, S.-K., Zhang, X., Zwiers, F. W., & Hegerl, G. C. (2011). Human contribution to more-intense precipitation extremes. *Nature*, *470*(7334), 378–381. https://doi.org/10.1038/nature09763

Mundhenk, B. D., Barnes, E. A., & Maloney, E. D. (2016). All-season climatology and variability of atmospheric river frequencies over the North Pacific. *Journal of Climate*, *29*(13), 4885–4903. https://doi.org/10.1175/jcli-d-15-0655.1

Mundhenk, B. D., Barnes, E. A., Maloney, E. D., & Baggett, C. F. (2018). Skillful empirical subseasonal prediction of landfalling atmospheric river activity using the Madden–Julian oscillation and quasi-biennial oscillation. *npj Climate and Atmospheric Science*, *1*(1), 20177. https://doi.org/10.1038/s41612-017-0008-2

Murakami, H. (2014). Tropical cyclones in reanalysis data sets. *Geophysical Research Letters*, *41*(6), 2133–2141. https://doi.org/10.1002/2014gl059519

Murakami, H. (2022). Substantial global influence of anthropogenic aerosols on tropical cyclones over the past 40 years. *Science Advances*, *8*(19), eabn9493. https://doi.org/10.1126/sciadv.abn9493

Murakami, H., Delworth, T. L., Cooke, W. F., Zhao, M., Xiang, B., & Hsu, P.-C. (2020). Detected climatic change in global distribution of tropical cyclones. *Proceedings of the National Academy of Sciences of the United States of America*, *117*(20), 10706–10714. https://doi.org/10.1073/pnas.1922500117

Murakami, H., Hsu, P.-C., Arakawa, O., & Li, T. (2014). Influence of model biases on projected future changes in tropical cyclone frequency of occurrence. *Journal of Climate*, *27*(5), 2159–2181. https://doi.org/10.1175/jcli-d-13-00436.1

Murakami, H., & Sugi, M. (2010). Effect of model resolution on tropical cyclone climate projections. *SOLA*, *6*, 73–76. https://doi.org/10.2151/sola.2010-019

Murakami, H., Vecchi, G. A., Underwood, S., Delworth, T. L., Wittenberg, A. T., Anderson, W. G., et al. (2015). Simulation and prediction of category 4 and 5 Hurricanes in the high-resolution GFDL HiFLOR coupled climate model. *Journal of Climate*, *28*(23), 9058–9079. https://doi.org/10.1175/jcli-d-15-0216.1

Nazarian, R. H., Vizzard, J. V., Agostino, C. P., & Lutsko, N. J. (2022). Projected changes in future extreme precipitation over the Northeast US in the NA-CORDEX ensemble. *Journal of Applied Meteorology and Climatology*, *61*(11), 1649–1668. https://doi.org/10.1175/jamc-d-22-0008.1

NCAR Research Data Archive. (2023). JRA-55: Japanese 55-year reanalysis [Dataset]. *NCAR Research Data Archive*. Retrieved from https://rda.ucar.edu/datasets/ds628.0/

Nellikkattil, A. B., Lee, J.-Y., Guan, B., Timmermann, A., Lee, S.-S., Chu, J.-E., & Lemmon, D. (2023). Increased amplitude of atmospheric rivers and associated extreme precipitation in ultra-high-resolution greenhouse warming simulations. *Communications Earth & Environment*, *4*(1), 313. https://doi.org/10.1038/s43247-023-00963-7

Ning, L., Riddle, E. E., & Bradley, R. S. (2015). Projected changes in climate extremes over the northeastern United States. *Journal of Climate*, *28*(8), 3289–3310. https://doi.org/10.1175/jcli-d-14-00150.1

O'Brien, T. A., Wehner, M. F., Payne, A. E., Shields, C. A., Rutz, J. J., Leung, L.-R., et al. (2022). Increases in future AR count and size: Overview of the ARTMIP tier 2 CMIP5/6 experiment. *Journal of Geophysical Research: Atmospheres*, *127*(6), e2021JD036013. https://doi.org/10.1029/2021jd036013

Olafdottir, H. K., Rootzen, H., & Bolin, D. (2021). Extreme rainfall events in the northeastern United States become more frequent with rising temperatures, but their intensity distribution remains stable. *Journal of Climate*, *34*, 8863–8877. https://doi.org/10.1175/jcli-d-20-0938.1

Patricola, C. M., & Wehner, M. F. (2018). Anthropogenic influences on major tropical cyclone events. *Nature*, *563*(7731), 339–346. https://doi.org/10.1038/s41586-018-0673-2

Payne, A. E., Demory, M.-E., Leung, L. R., Ramos, A. M., Shields, C. A., Rutz, J. J., et al. (2020). Responses and impacts of atmospheric rivers to climate change. *Nature Reviews Earth & Environment*, *1*(3), 143–157. https://doi.org/10.1038/s43017-020-0030-5

Picard, C. J., Winter, J. M., Cockburn, C., Hanrahan, J., Teale, N. G., Clemins, P. J., & Beckage, B. (2023). Twenty-first century increases in total and extreme precipitation across the Northeastern USA. *Climatic Change*, *176*(6), 72. https://doi.org/10.1007/s10584-023-03545-w

Reed, K. A., & Chavas, D. R. (2015). Uniformly rotating global radiative-convective equilibrium in the Community Atmosphere Model, version 5. *Journal of Advances in Modeling Earth Systems*, *7*(4), 1938–1955. https://doi.org/10.1002/2015ms000519

Roberts, M. J., Camp, J., Seddon, J., Vidale, P. L., Hodges, K., Vanniere, B., et al. (2020a). Impact of model resolution on tropical cyclone simulation using the HighResMIP–PRIMAVERA multimodel ensemble. *Journal of Climate*, *28*(7), 2557–2583. https://doi.org/10.1175/jcli-d-19-0639.1

Roberts, M. J., Camp, J., Seddon, J., Vidale, P. L., Hodges, K., Vannière, B., et al. (2020b). Projected future changes in tropical cyclones using the CMIP6 HighResMIP multimodel ensemble. *Geophysical Research Letters*, *47*(14), e2020GL088662. https://doi.org/10.1029/2020gl088662

Roberts, M. J., Vidale, P. L., Mizielinski, M. S., Demory, M.-E., Schiemann, R., Strachan, J., et al. (2015). Tropical cyclones in the UPSCALE ensemble of high-resolution global climate models. *Journal of Climate*, *28*(2), 574–596. https://doi.org/10.1175/jcli-d-14-00131.1

Rutz, J. J., Shields, C. A., Lora, J. M., Payne, A. E., Guan, B., Ullrich, P., et al. (2019). The Atmospheric River Tracking Method Intercomparison Project (ARTMIP): Quantifying uncertainties in atmospheric river climatology. *Journal of Geophysical Research: Atmospheres*, *124*(24), 13777–13802. https://doi.org/10.1029/2019jd030936

Schiemann, R., Vidale, P. L., Shaffrey, L. C., Johnson, S. J., Roberts, M. J., Demory, M.-E., et al. (2018). Mean and extreme precipitation over European river basins better simulated in a 25 km AGCM. *Hydrology and Earth System Sciences*, *22*(7), 3933–3950. https://doi.org/10.5194/hess-22-3933-2018

Shaevitz, D. A., Camargo, S. J., Sobel, A. H., Jonas, J. A., Kim, D., Kumar, A., et al. (2014). Characteristics of tropical cyclones in high-resolution models in the present climate. *Journal of Advances in Modeling Earth Systems*, *6*(4), 1154–1172. https://doi.org/10.1002/2014ms000372

Slinskey, E. A., Loikith, P. C., Waliser, D. E., Guan, B., & Martin, A. (2020). A climatology of atmospheric rivers and associated precipitation for the seven U.S. National Climate Assessment Regions. *Journal of Hydrometeorology*, *21*(11), 2439–2456. https://doi.org/10.1175/jhm-d-20-0039.1

Smith, J. A., Villarini, G., & Baeck, M. L. (2011). Mixture distributions and the hydroclimatology of extreme rainfall and flooding in the eastern United States. *Journal of Hydrometeorology*, *12*(2), 294–309. https://doi.org/10.1175/2010jhm1242.1

Sobel, A. H., Wing, A. A., Camargo, S. J., Patricola, C. M., Vecchi, G. A., Lee, C., & Tippett, M. K. (2021). Tropical cyclone frequency. *Earth's Future*, *9*(12), e2021EF002275. https://doi.org/10.1029/2021ef002275

Stansfield, A. M., Reed, K. A., & Zarzycki, C. M. (2020). Changes in precipitation from North Atlantic tropical cyclones under RCP scenarios in the variable-resolution community atmosphere model. *Geophysical Research Letters*, *47*(12), e2019GL086930. https://doi.org/10.1029/2019gl086930

Stansfield, A. M., Reed, K. A., Zarzycki, C. M., Ullrich, P. A., & Chavas, D. R. (2020). Assessing tropical cyclones' contribution to precipitation over the eastern United States and sensitivity to the variable-resolution domain extent. *Journal of Hydrometeorology*, *21*(7), 1425–1445. https://doi.org/10.1175/jhm-d-19-0240.1

Sun, Q., Miao, C., Duan, Q., Ashouri, H., Sorooshian, S., & Hsu, K. (2018). A review of global precipitation data sets: Data sources, estimation, and intercomparisons. *Reviews of Geophysics*, *56*(1), 79–107. https://doi.org/10.1002/2017rg000574

Teale, N., & Robinson, D. A. (2020). Patterns of water vapor transport in the eastern United States. *Journal of Hydrometeorology*, *21*(9), 2123–2138. https://doi.org/10.1175/jhm-d-19-0267.1

Ting, M., Kossin, J. P., Camargo, S. J., & Li, C. (2019). Past and future hurricane intensity change along the U.S. East Coast. *Scientific Reports*, *9*(1), 7795. https://doi.org/10.1038/s41598-019-44252-w

Touma, D., Stevenson, S., Camargo, S. J., Horton, D. E., & Diffenbaugh, N. S. (2019). Variations in the intensity and spatial extent of tropical cyclone precipitation. *Geophysical Research Letters*, *46*(23), 13992–14002. https://doi.org/10.1029/2019gl083452

Tseng, K., Johnson, N. C., Kapnick, S. B., Cooke, W., Delworth, T. L., Jia, L., et al. (2022). When will humanity notice its influence on atmospheric rivers? *Journal of Geophysical Research: Atmospheres*, *127*(9), e2021JD036044. https://doi.org/10.1029/2021jd036044

Ullrich, P. A., & Zarzycki, C. M. (2017). TempestExtremes: A framework for scale-insensitive pointwise feature tracking on unstructured grids. *Geoscientific Model Development*, *10*(3), 1069–1090. https://doi.org/10.5194/gmd-10-1069-2017

Van der Wiel, K., Kapnick, S. B., Vecchi, G. A., Cooke, W. F., Delworth, T. L., Jia, L., et al. (2016). The resolution dependence of contiguous U.S. precipitation extremes in response to CO_2 forcing. *Journal of Climate*, *29*(22), 7991–8012. https://doi.org/10.1175/jcli-d-16-0307.1

Vannière, B., Demory, M.-E., Vidale, P. L., Schiemann, R., Roberts, M. J., Roberts, C. D., et al. (2019). Multi-model evaluation of the sensitivity of the global energy budget and hydrological cycle to resolution. *Climate Dynamics*, *52*(11), 6817–6846. https://doi.org/10.1007/s00382-018-4547-y

Vecchi, G. A., Delworth, T. L., Murakami, H., Underwood, S. D., Wittenberg, A. T., Zeng, F., et al. (2019). Tropical cyclone sensitivities to CO_2 doubling: Roles of atmospheric resolution, synoptic variability and background climate changes. *Climate Dynamics*, *53*(9–10), 5999–6033. https://doi.org/10.1007/s00382-019-04913-y

Wang, S., Murakami, H., & Cooke, W. F. (2023). Anthropogenic forcing changes coastal tropical cyclone frequency. *npj Climate and Atmospheric Science*, *6*(1), 187. https://doi.org/10.1038/s41612-023-00516-x

Wehner, M. F., Reed, K. A., Li, F., Prabhat, Bacmeister, J., Chen, C.-T., et al. (2014). The effect of horizontal resolution on simulation quality in the Community Atmospheric Model, CAM5.1. *Journal of Advances in Modeling Earth Systems*, *6*(4), 980–997. https://doi.org/10.1002/2013ms000276

Wehner, M. F., Smith, R. L., Bala, G., & Duffy, P. (2010). The effect of horizontal resolution on simulation of very extreme US precipitation events in a global atmosphere model. *Climate Dynamics*, *34*(2–3), 241–247. https://doi.org/10.1007/s00382-009-0656-y

Wright, D. B., Knutson, T. R., & Smith, J. A. (2015). Regional climate model projections of rainfall from U.S. landfalling tropical cyclones. *Climate Dynamics*, *45*(11–12), 3365–3379. https://doi.org/10.1007/s00382-015-2544-y

Zhang, G., Murakami, H., Knutson, T. R., Mizuta, R., & Yoshida, K. (2020). Tropical cyclone motion in a changing climate. *Science Advances*, *6*(17), eaaz7610. https://doi.org/10.1126/sciadv.aaz7610

Zhao, M. (2020). Simulations of atmospheric rivers, their variability, and response to global warming using GFDL's new high-resolution general circulation model. *Journal of Climate*, *33*(23), 10287–10303. https://doi.org/10.1175/jcli-d-20-0241.1

Zhao, M. (2022). A study of AR-, TS-, and MCS-associated precipitation and extreme precipitation in present and warmer climates. *Journal of Climate*, *35*(2), 479–497. https://doi.org/10.1175/jcli-d-21-0145.1

Zhao, M., Golaz, J.-C., Held, I. M., Guo, H., Balaji, V., Benson, R., et al. (2018). The GFDL global atmosphere and land model AM4.0/LM4.0: 1. Simulation characteristics with prescribed SSTs. *Journal of Advances in Modeling Earth Systems*, *10*(3), 691–734. https://doi.org/10.1002/2017ms001208